9 Principles of Spike Train Analysis

Fabrizio Gabbiani and Christof Koch

9.1 Introduction

Experiments in sensory neurophysiology often record action potential arrival times of nerve cells resulting from spontaneous or stimulus-evoked activity. When all action potentials are taken to be identical and only their localized times of occurrence are considered, one obtains a discrete series of time events, $\{t_1, \ldots t_n$, where t_i = time of arrival of the ith spike$\}$, characterizing the spike train. It is this series of events that is transmitted down the axon to all of the cell's targets and that contains most, if not all, of the information the cell is conveying.

Most of this information is neglected when studying the *average rate*, the number of action potentials over some suitable interval usually lasting a fraction of a second or longer, as the relevant variable characterizing the neuronal response. Recently, the *temporal coding* of information in the patterns of spikes, both in the single cell as well as between multiple cells, has received renewed attention. The broad idea that spike timing, in particular across an ensemble of cells, plays an important role in encoding various aspects of the stimulus is supported by experiments in a variety of sensory systems such as locust olfaction, electric fish electrosensation, cat vision and olfaction, as well as monkey vision and audition (Chung, Raymond, and Lettvin 1970; Freeman 1975; Abeles 1990; Strehler and Lestienne 1986; Bialek et al. 1991; Eskandar, Richmond, and Optican 1992; Singer and Gray 1995; Decharms and Merzenich 1996; Laurent 1996; Wehr and Laurent 1996; Gabbiani et al. 1996; Lisman 1997).

The characteristics of the neuronal code are closely linked to the seemingly *stochastic* or *random* character of neuronal firing. Because little or no information can be encoded into a stream of completely regularly spaced action potentials, this raises the questions of how variable neuronal firing really is and what the relation is between variability and the neural code. It is the mathematical theory of stochastic point processes and the field of statistical signal processing that offer us the adequate tools for attacking these questions.

This chapter surveys a selection of such tools, starting with the classical interspike interval histograms commonly used in neurophysiological studies. The methods presented here are intended to shed additional light on two aspects of neuronal signal processing: (1) the integrative mechanisms underlying the activity of nerve cells; (2) the nature and reliability of stimulus encoding in neuronal spike trains.

To address these aspects and illustrate the methods presented here, we study the encoding of various signals in spike trains of certain simplified single-cell models, in

particular integrate-and-fire neurons and Poisson spike train generators. This allows us to investigate in a controlled manner the effect of several biophysical parameters such as refractoriness or mean firing rate on the encoding of various signals. These models are described in detail in section 9.2. They can all be modeled using the MATLAB routines provided by us (see below and chapter appendix B).

Section 9.3 introduces the classical measure of variability associated with interspike interval distributions: the coefficient of variation, C_V. Its dependence on various biophysical and stimulus parameters is then investigated. In section 9.4, a different and complementary measure of variability of the neuronal response, the ratio of the variance to the mean spike count in a fixed time interval, F, is introduced. This measure plays an important role in determining the accuracy with which information can be conveyed in the mean spike count, as explained in section 9.5. Sections 9.6–9.7 are devoted to the analysis of information encoded in the timing of neuronal spiking. In section 9.6, the autocorrelation function and power spectrum of the time series of action potential events are defined. While the power spectrum is a measure of the frequency content of the spike train and can, under some assumptions, reflect to processing performed by the neuron on its input stimuli, it is also influenced by intrinsic properties of the neuron, like its refractory period or its tendency to fire regularly. The autocorrelation function, in turn, translates these properties in the time domain. Section 9.7 introduces a method that allows to directly assess the accuracy of the information transmitted by a neuron about a time-varying stimulus by estimating the stimulus from the spike train.

Increasingly fast computers and the availability of comprehensive software packages with practical graphical interfaces has made the analysis of neuronal data using the methods presented here more rapid and convenient. One of these packages, MATLAB, is well suited for such numerical work and was used to analyze our data. The corresponding programs (MATLAB M-files) can be freely accessed and downloaded from our web site (see chapter appendix B for a more detailed description as well as http://www.klab.caltech.edu/~gabbiani/signproc.html). All of the functions and spike generation models used in the following pages are defined within a simple and intuitive programming environment, based on the dynamical system simulation package of MATLAB called "Simulink." We also provide several tutorials that will allow the interested reader to directly generate and analyze the data from our models (as well as more elaborate variants, which are only briefly mentioned here) and to further explore topics not covered in this chapter. (For an early review and references on the subject of this chapter, see Schmitt 1970, chapters 51–58; see also Rieke et al. 1996.)

9.2 Models

We start by introducing several simplified models that will be used to illustrate the analysis methods explored in the following sections. We do not intend to perform biophysically detailed modeling of single neurons here (this subject is covered in chapters 3–6, this volume). The goal of this chapter is to incorporate some basic biophysical properties of real nerve cells, such as refractoriness, spike train variability or bursting, into idealized single-cell models, along with plausible processing schemes for input signals and to analyze the properties of the resulting spike trains. While none of the models described below can faithfully reproduce all the properties of a given neuronal spike train, each one of them has been shown in several instances to successfully capture at least some of them.

9.2.1 Perfect Integrate-and-Fire Neuron

We turn to a very simple, but quite powerful model of a spiking cell with a long and distinguished history, first investigated by Lapicque (1907, 1926). It is known as the "integrate-and-fire model" (Stein 1967a, 1967b; Knight 1972a; Tuckwell 1988) and assumes that the neuron integrates its inputs and generates a spike when a fixed voltage threshold is reached:

$$C_m \cdot \frac{dV_m}{dt} = I(t), \tag{9.1}$$

where $I(t)$ is the input current, integrated to yield the membrane voltage $V_m(t)$. In eq. 9.1, the resting membrane potential has been set to zero for convenience and the constant C_m represents the capacity of the model cell. With the help of an initial condition, such as $V_m(0) = 0$, eq. 9.1 specifies the evolution of the membrane potential in the subthreshold domain (figure 9.1).

A spike is generated each time that $V_m(t)$ reaches the threshold V_{th} and the membrane voltage is reset to zero immediately after a spike. Thus the successive times, t_i, of spike occurrence are determined recursively from the equation

$$\int_{t_i}^{t_{i+1}} I(t)\, dt = C_m V_{th}. \tag{9.2}$$

The response of such a model to a positive constant current step has the following characteristics: (1) the firing rate, f, is linearly related to the magnitude of the input current: $f(I) = I/C_m V_{th}$, in other words, the frequency-current or f-I curve is linear (see figure 9.2); (2) arbitrarily small input currents eventually lead to a spike, that is,

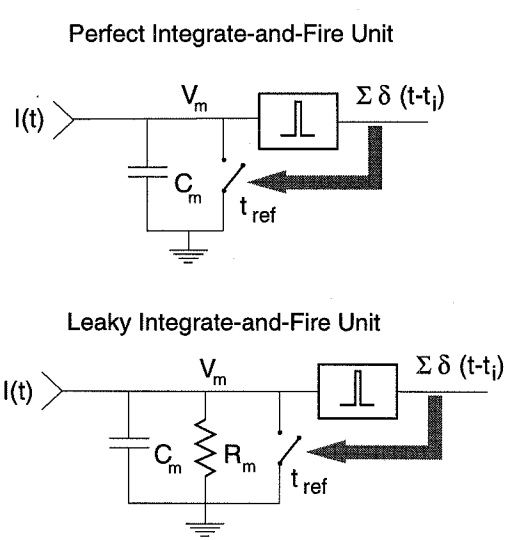

Figure 9.1
Two variants of integrate-and-fire "units." Common to both are passive integration within a single compartment for the subthreshold domain and a voltage threshold V_{th}. Whenever the membrane potential V_m reaches V_{th}, a pulse is generated and the circuit is short-circuited. For a duration t_{ref} following spike generation, any input $I(t)$ is shunted to ground (corresponding to an absolute refractory period). (A) Perfect or nonleaky integrate-and-fire model contains but a capacitance. (B) Leaky or forgetful integrate-and-fire unit accounts for the decay of the membrane potential by an additional component, a leak resistance R_m.

the model never "forgets" the occurrence of an input; and (3) the corresponding output spike train is perfectly regular.

Several simple modifications of this basic model lead to very different behaviors.

9.2.2 Refractory Period

In real neurons, the dynamic firing range is limited by the biophysical properties of the ionic membrane conductances responsible for action potential generation. In particular, neurons do not fire at arbitrarily high rates because sodium channels need to recover from inactivation between two action potentials. As a first approximation, this constraint can be implemented in the preceding model by assuming that after a spike the neuron is entirely inactive for a fixed period of time, t_{ref} (the absolute refractory period or dead time), before it resumes normal function. That is, for a fixed time after spike generation, all input current is shunted off. Such a refractory period limits the firing frequency to $f_{max} = 1/t_{ref}$ and thus introduces a nonlinear saturation in the f-I curve for large inputs:

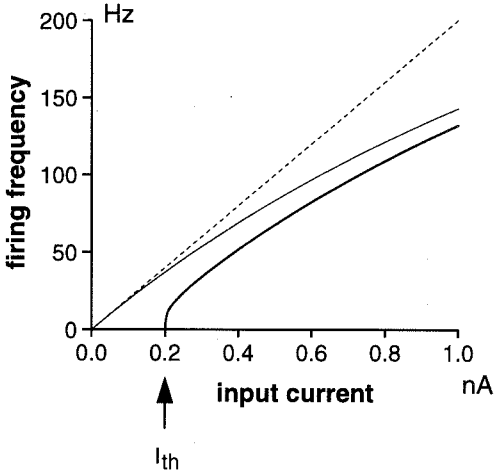

Figure 9.2
Graph of f-I curves for an integrate-and-fire model without and with refractory period (thin solid line and dashed line, respectively) and for a leaky integrate-and-fire model with refractory period (thick solid line). The f-I curve of the (leaky) integrate-and-fire neuron with refractory period saturates for high input currents at the inverse of the absolute refractory period (here 5 msec). The leaky integrate-and-fire model will not respond to currents less than I_{th} (arrow) because of its tendency to "forget" inputs, while for high currents its f-I curve becomes similar to the one of the perfect integrate-and-fire model. This and all following figures were generated using the MATLAB routines described in chapter appendix B and made available at our web site.

$$f(I) = \frac{I}{C_m V_{th} + t_{ref} \cdot I} \tag{9.3}$$

(see figure 9.2).

9.2.3 Leaky Integrate-and-Fire Neuron

The integrate-and-fire neuron considered above will sum linearly two subthreshold inputs irrespective of their temporal separation because it does not gradually forget the occurrence of events over time. A more realistic behavior is obtained by introducing a leak term in the dynamics of the subthreshold membrane voltage:

$$C_m \frac{dV_m}{dt} = I(t) - \frac{V_m}{R_m}, \tag{9.4}$$

driving it toward its resting value, $V_m = 0$. The leak term is characterized by the resistance to current flowing out of the cell, R_m (figure 9.1).

In response to a constant current pulse I, this leaky integrate-and-fire model will relax exponentially toward a steady-state voltage $V_m = IR_m$:

$$V_m(t) = IR_m(1 - e^{-t/\tau_m}), \tag{9.5}$$

with time constant $\tau_m = R_m C_m$. Thus the minimal threshold current required to drive the cell to threshold is $I_{th} = V_{th}/R_m$ (also known as the "rheobase current"). The corresponding f-I curve is given by

$$f(I) = \begin{cases} 0 & \text{if } I \leq I_{th}, \\ \left[t_{ref} - \tau_m \log\left(1 - \frac{V_{th}}{IR_m}\right)\right]^{-1}, & I > I_{th}. \end{cases} \tag{9.6}$$

For large input currents, the leak term in eq. 9.4 does not contribute significantly; the f-I curve of eq. 9.3 is recovered (by using $\log(1 - x) \sim -x$, for $|x| \ll 1$ in eq. 9.6; see figure 9.2).

Due to the presence of the leak term, integrate-and-fire models have been difficult to fully characterize analytically (Poggio and Torre 1977) but have also been surprisingly successful in describing neuronal excitability. They have been applied to model the firing behavior of numerous cell types: neurons in the *Limulus* eye (Knight 1972b), α-motoneurons (Calvin and Stevens 1968), neurons in the visual system of the housefly (Gestri, Masterbroek, and Zaagman 1980), and cortical cells (Softky and Koch 1993; Troyer and Miller 1997), among others.

We will mostly consider the case of a perfect integrator model because it allows us to write down closed-form solutions for many variables of interest. However, the behavior of the leaky integrator will approach that of the perfect integrate-and-fire model if the average interspike interval is short compared to the time constant τ_m.

9.2.4 Poisson Spike Trains and Integrate-and-Fire Neurons with Random Threshold

While some neurons fire regularly in response to injected suprathreshold currents, many neurons show a considerable degree of variability in their sequence of action potentials, in contrast to (leaky) integrate-and-fire neurons. Irregular firing is particularly pronounced in the case of recordings carried out in vivo, rather than in brain slices or in cultured cells (Holt et al. 1996). We here consider a class of models able to produce irregular spike trains. The following description is phenomenological; possible causes for this variability will be considered more closely in section 9.3.

An irregular response to a constant current pulse can be obtained in a model that generates a spike at an average rate of $f = I/C_m V_{th}$, but in such a way that (1) every spike is generated randomly, (2) independently of other spikes and (3) with a uniform probability of occurrence in time. The resulting spike sequence is called "a Poisson spike train" and is highly variable because of the complete independence between the time of occurrence of neighboring spikes. Neuronal response variability is often

compared to the variability of a Poisson spike train because of its simplicity. However, real spike trains usually have interspike intervals that are not independent from each other but that may depend on the preceding interspike intervals.

As a consequence of properties 1–3, the interspike interval distribution of a Poisson spike train is exponentially distributed with probability density

$$p(t) = (1/\bar{t})e^{-t/\bar{t}}, \tag{9.7}$$

where $\bar{t}$ is the mean interspike interval (figure 9.3A). The density function $p(t)$ is obtained experimentally by binning consecutive interspike intervals from spike trains, as in figure 9.3. In this guise it is called the "interspike interval" (ISI) histogram.

Because in an integrate-and-fire neuron the mean interspike interval is proportional to the voltage threshold, Poisson spike trains can be obtained from an integrate-and-fire neuron by reseting the threshold after each spike to a new random value according to the distribution $p(V) = (1/V_{th})e^{-V/V_{th}}$. The voltage V_{th} now denotes the mean value of the distribution $p(V)$. Similarly, by assuming that the random threshold is distributed according to a gamma distribution of order n,

$$p_n(V) = \frac{c_n V^{n-1}}{V_{th}^{n-1}} e^{-nV/V_{th}}, \tag{9.8}$$

with

$$c_n = \frac{n^n}{(n-1)!}\frac{1}{V_{th}}, \tag{9.9}$$

one obtains increasingly regular spike trains in response to a constant current injection as n increases. The case $n = 1$ corresponds to Poisson spike trains and in the limit $n \to \infty$, the usual integrate-and-fire neuron is recovered. The resulting interspike intervals are gamma distributed around their mean value (figure 9.3).

It could be argued that a random voltage threshold is not a very realistic physiological feature. After all, noise in the spiking mechanism is seldomly observed in real neurons (Calvin and Stevens 1968; Mainen and Sejnowski 1995), although, in the case of a perfect or nonleaky integrate-and-fire model, a random threshold can be shown to be equivalent to a random input current (Gestri, Masterbroek, and Zaagman 1980).

This point is most easily illustrated by considering an integrate-and-fire neuron that receives as input Poisson-distributed current pulses of size I_0 at an average frequency f_0 (as in figure 9.4). If n_{th} is the number of inputs needed to fire the cell (i.e., n_{th} is the smallest integer larger than $C_m V_{th}/I_0$; see eq. 9.1) then the average firing rate of the

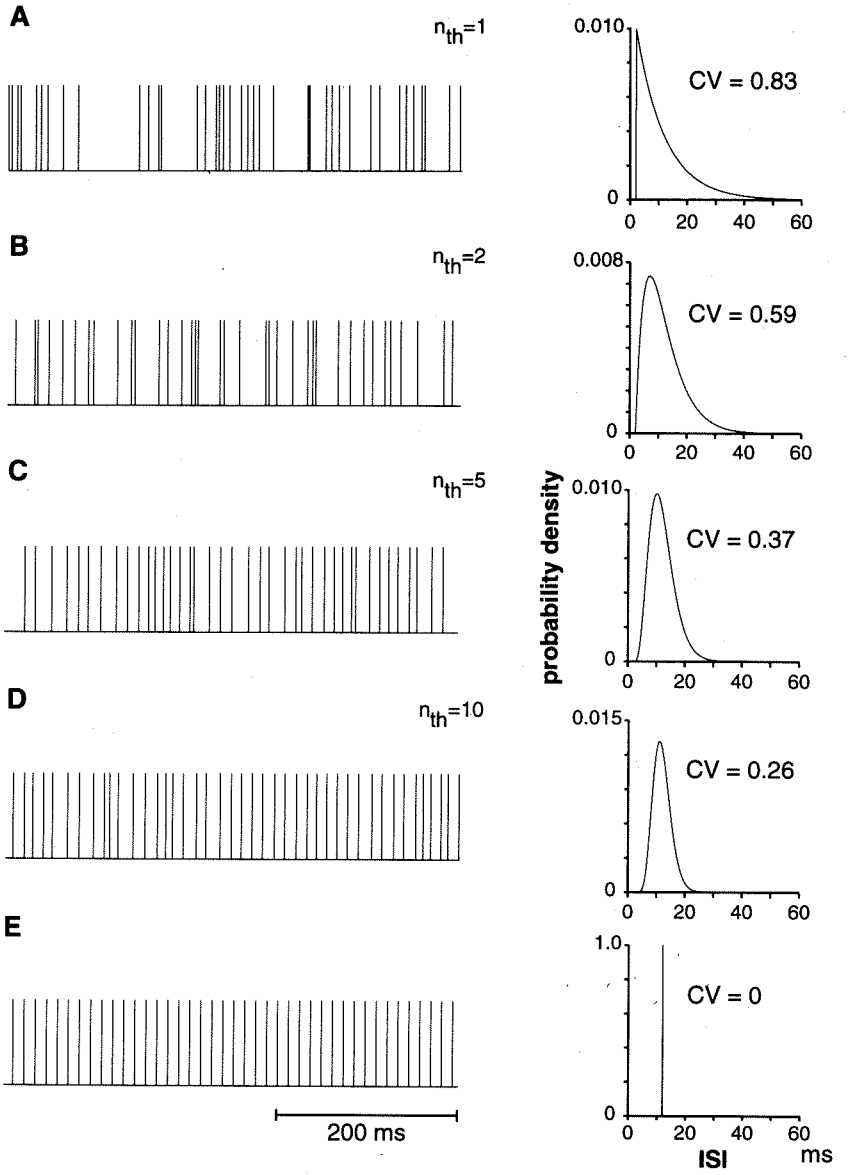

Figure 9.3
Sample spike trains and interspike interval (ISI) distributions from various models in response to a constant current input into a perfect integrator model. All models have an absolute refractory period of 2 msec and a mean firing rate of 83 Hz. (A) Poisson-distributed (i.e., exponential) random voltage threshold yields the most irregular spike train and an exponential ISI distribution. In the absence of a refractory period, C_V would be 1. (B–D) Gamma-distributed random thresholds of order 2, 5, and 10 yield increasingly regular ISI distributions, which are gamma-distributed of order 2, 5, and 10, respectively. (E) Integrate-and-fire model yields a perfectly regular spike train, corresponding to the limit $n \rightarrow \infty$. Spike trains with identical properties can be generated by a perfect integrator with fixed voltage threshold, Poisson-distributed synaptic input and, in panel A, $n_{th} = 1$ (i.e., each input triggers one output spike), in panels B–D, $n_{th} = 2, 5,$ and 10 and, in panel E, a constant input current. The rate of the input Poisson process is adjusted to obtain the same mean firing rate in all cases.

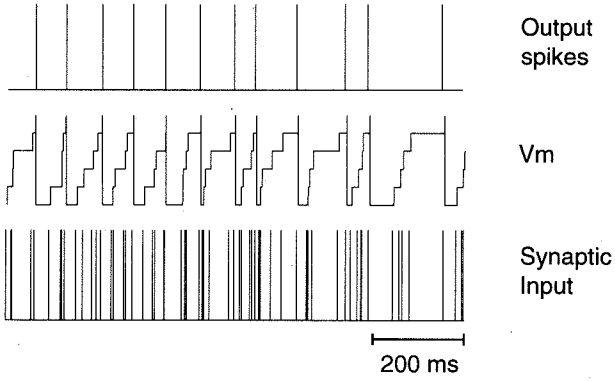

Figure 9.4
Perfect or nonleaky integrate-and-fire model averages out noise by summing its inputs until V_{th} is reached. While the Poisson synaptic input (lower trace) is highly irregular, the time to the next spike is averaged out in the membrane voltage (V_m, middle trace), yielding a more regular output spike train (top trace). In this example, $n_{th} = 5$ inputs are needed to reach threshold, thus yielding a spike train with gamma-distributed ISI distribution of order 5 (see figure 9.3C), whereas the synaptic input ISI distribution is exponential (see figure 9.3A).

model will be f_0/n_{th}. The distribution of spikes can be shown (Tuckwell 1988) to correspond to a gamma distribution of order n_{th}, identical to the interspike interval distribution considered in eq. 9.8 (figure 9.3; Tuckwell 1988).

Indeed, the statistical properties of the output spikes of both models are identical. That is, Poisson-distributed inputs into an integrator unit that requires n_{th} synaptic inputs to reach a fixed threshold V_{th} is equivalent to injecting a constant current $f_0 I_0$ into an integrator unit whose voltage threshold is distributed according to eq. 9.8 and where this constant input triggers the output spikes. Expressing the variability in terms of a random threshold distribution has mathematical and numerical advantages (see chapter appendix B). For example, the case of an *inhomogeneous Poisson process*, in which spikes are generated independently of each other with a time-varying rate $\lambda(t)$, is again equivalent to the case of injecting a deterministic current proportional to $\lambda(t)$ into the unit and having a random threshold of the form expressed in eq. 9.8.

9.3 Interspike Interval Distribution and Coefficient of Variation

The variability of a neuronal spike train is an important indicator of the type of processing a neuron performs on its synaptic inputs. The simplest measure of variability is the coefficient of variation of the interspike interval distribution, a dimensionless number defined as the standard deviation σ_t of the interspike interval

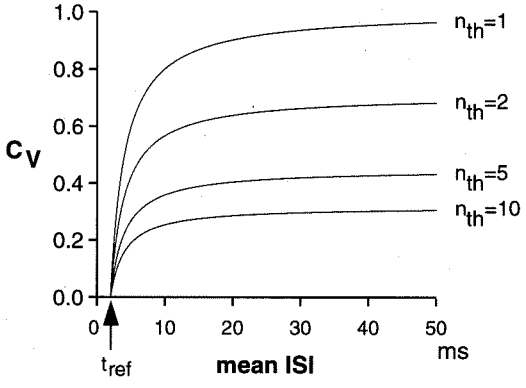

Figure 9.5
Coefficient of variation of an integrate-and-fire neuron with a 2 msec refractory period as a function of the mean ISI. The different curves denote the number of inputs n_{th} summed by the model to reach the voltage threshold. As the firing frequency increases toward the limit imposed by the refractory period t_{ref} (arrow), the spike trains becomes more regular ($C_V \to 0$ for mean ISI $\to$ 2 msec). In other words, the refractory period exerts a regularizing effect on the spike train.

distribution normalized by the mean interspike interval $\bar{t}$:

$$C_V = \frac{\sigma_t}{\bar{t}}, \tag{9.10}$$

with

$$\bar{t} = \int_0^\infty t p(t)\, dt, \quad \text{and } \sigma_t^2 = \int_0^\infty (t - \bar{t})^2 p(t)\, dt, \tag{9.11}$$

where $p(t)$ is the probability density distribution of the interspike intervals. The coefficient of variation is equal to 1 for Poisson spike trains, since $\sigma_t = \bar{t}$, while for a gamma distribution of order n, $\sigma_t^2 = \bar{t}^2/n$ and $C_V = 1/\sqrt{n}$ (see eq. 9.8).

In other words, integrating over a large number of small inputs gives rise to very regular output spikes (figures 9.3–9.5). In the limit of an integrate-and-fire neuron under constant current input, $C_V \to 0$. Conversely, a neuron that is sensitive to a small number of random inputs is expected to generate very irregular spike trains. In real nerve cells, further potential sources of variability include the stochastic nature of synaptic transmission, nonlinear amplification of synaptic inputs by active dendritic conductances and network effects due to the interconnectivity of nerve cells (Softky and Koch 1993; Allan and Stevens 1994; Stuart and Sakmann 1994; van Vreeswijk and Sompolinsky 1996).

A refractory period lowers the C_V at high firing rates when it tends to force regularity in the interspike interval duration. In the ideal case of an absolute refractory period, the interspike interval probability density will simply be shifted to the right of the time axis, $p(t) \rightarrow p_{ref}(t) = p(t - t_{ref})$ and the new coefficient of variation is

$$C_{V_{ref}} = (1 - t_{ref}/\bar{t})C_V, \tag{9.12}$$

to that $C_{V_{ref}} \rightarrow 0$ as $\bar{t} \rightarrow t_{ref}$ (figures 9.3 and 9.5).

The time constant of integration of a leaky integrate-and-fire neuron will affect the coefficient of variation in a different way. If $n_{th} > 1$ coincident inputs are needed to fire the cell, a large τ_m will regularize the spike train by averaging the arrival of synaptic inputs over time, whereas a short τ_m will increase the sensitivity to coincident inputs and thus boost up variability.

In all of these examples, $C_V \leq 1$, with the upper bound given by a pure Poisson process, although in many instances interspike interval distributions of real neurons have C_V values greater than 1. This can be achieved in a Poisson neuron by assuming that the current (or the rate) driving the model is itself random in time. The resulting spike trains are termed *doubly stochastic Poisson* in the mathematical and engineering literature (Saleh 1978; Peřina 1985) because of the dual source of variability arising in the current and the spike generation mechanism. This is illustrated, for example, in a model that successfully describes several properties of retinal ganglion cell spike trains at low light levels (Saleh and Teich 1985). In this limit, the distribution of photons absorbed at the retina is expected to be Poisson. If each photon results in a slowly decaying input current to a ganglion cell that causes on average two output spikes per incoming photon (see figure 9.6A), then the interspike interval distribution of the model will have a C_V greater than 1 (figure 9.6B). The cause of this additional variability lies in the random number of spikes generated for each incoming Poisson pulse.

Other cell classes respond to inputs with a *burst* of spikes, that is, a small number of spikes separated by short interspike intervals. Several further special models and techniques have been developed to analyze the variability of such bursting cells (Bair et al. 1994; Franklin and Bair 1995; Holt et al. 1996).

9.4 Spike Count Distribution and Fano Factor

Although the C_V yields a useful measure of short-term variability, because this measure is obtained from the interspike interval distribution, it yields a complete characterization of variability only if the occurrence of a spike depends exclusively on the

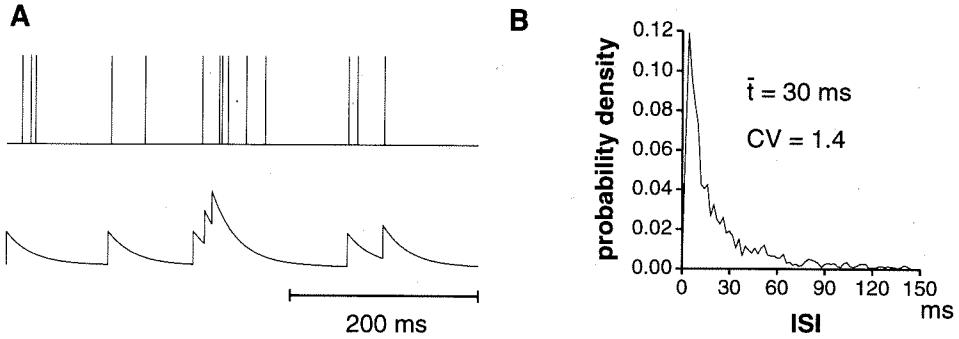

Figure 9.6
(A) Sample input current and spike train for the retinal ganglion cell model described in the main text, based on a doubly stochastic Poisson process. (B) Because of the added source of variability in the input current, the ISI distribution is more irregular than the one associated with a Poisson model (for which we would obtain $C_V = 1$).

time of the previous spike and not further on the past history of the spike train. This is the case for the Poisson- and gamma-distributed spike trains of figure 9.3; such spike trains are said to be generated by a *renewal process*. By definition, successive intervals between the spikes of a renewal process are independent (Cox 1962; Cox and Lewis 1966). Equivalently, the time of occurrence of a spike depends only on the previous one.

Information on variability beyond the first interspike interval can be gleaned from the distribution of spike counts measured over a time period of length T. To illustrate how the variability observed in the interspike intervals translates into variability of the spike count, we return to the examples of last section. For a Poisson spike train with mean firing rate $f = 1/\bar{t}$, the probability $p(n)$ of obtaining n spikes in the observation window T is

$$p(n) = \frac{(fT)^n e^{-fT}}{n!} \tag{9.13}$$

and is plotted in figure 9.7A.

For the model of retinal ganglion cell firing considered above, spike generation can be approximatively described as a cascade of two Poisson processes: the first one represents the absorption of photons at the retina and the second one the random generation of two spikes (on average) for each such photon.[1] The resulting spike count distribution (called a "Neyman type-A distribution"; see figure 9.7A; Teich 1981) is broader than a Poisson distribution of identical mean, consistent with the

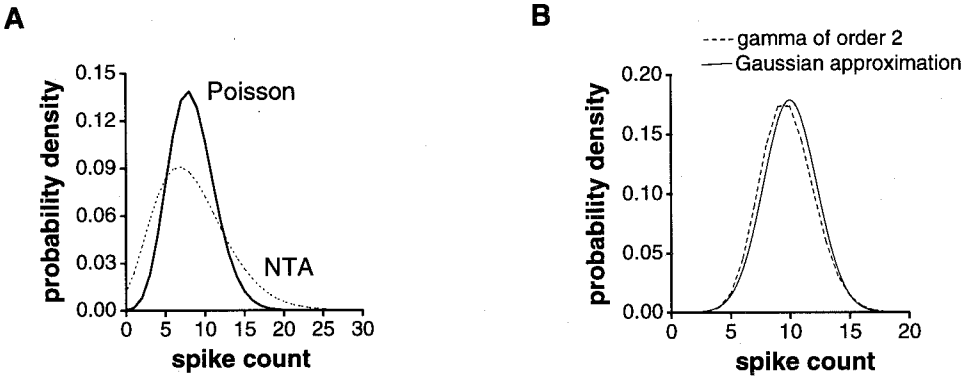

Figure 9.7
(A) Comparison of a Poisson (thick solid line) and Neyman type-A distribution (NTA, dotted line) of spike counts. The means of the two distributions are identical (8.35 spikes), but the variance of the NTA distribution is larger than the mean (the effective multiplication parameter k is equal to 1.45 in this example). (B) Spike count distribution (dashed line) obtained from a spike train with a gamma distributed ISI of order 2 (see figure 9.3B). The mean firing rate is $f = 50$ Hz and $T = 200$ msec. The corresponding Gaussian approximation (solid line, see main text) is already very good, even though only 10 spikes are expected in this period.

higher variability observed in the interspike interval distribution ($C_V > 1$; figure 9.6B).

The variability in the spike count distribution is most conveniently characterized by the ratio of the variance, $V(T)$, to the mean, $N(T)$, of $p(n)$:

$$F(T) = \frac{V(T)}{N(T)} \quad \text{(in units of spk)}. \tag{9.14}$$

This quantity is called the "index of dispersion" or "Fano factor." For a Poisson spike train, we obtain from eq. 9.13: $N(T) = fT$, $V(T) = fT$ and therefore $F(T) = 1$, independent of the duration T. For the Neyman type-A distribution, if we let f_{ph} denote the rate of incoming photons and k, the effective number of spikes per photon, then $N(T) = kf_{ph}T$, $V(T) = (k+1)f_{ph}T$ and therefore, $F(T) = 1 + k > 1$. Conversely, spike trains that are more regular than Poisson will have an index of dispersion smaller than 1. This is illustrated in figure 9.8 for a Poisson spike train with refractory period (Müller 1974) and for a gamma distribution of order 2 (Cox and Lewis 1966). In this latter case,

$$N(T) = \frac{T}{\bar{t}}, \quad V(T) = \frac{T}{2\bar{t}} + \frac{1}{8}(1 - e^{-4T/\bar{t}}), \tag{9.15}$$

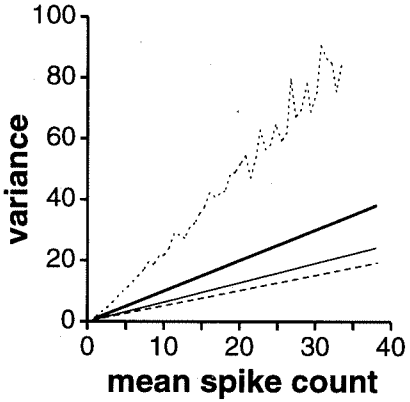

Figure 9.8
Variance as a function of mean spike count in several examples (the slope of these lines is the Fano factor of eq. 9.14). The curve with largest variance (dotted line) corresponds to the retinal ganglion cell model illustrated in figure 9.6 and was obtained by simulation. For a given mean spike count, the curve's variance is higher than the variance of a Poisson spike train (thick solid line), which has unit slope; that is, the variance increases as the mean number of spikes. Adding a 2 msec refractory period to the Poisson model (thin solid line) regularizes the spike count distribution, while the variance of a model with gamma-distributed ISI of order 2 (dashed line, see figure 9.3B) is only half of the mean spike count.

so that

$$F(T) = \frac{1}{2} + \frac{\bar{t}}{8T}(1 - e^{-4T/\bar{t}}). \tag{9.16}$$

While, for very small observation intervals, F converges to unity as in a standard Poisson process, for $T \to \infty$, F converges to 1/2.

9.4.1 Relationship between Coefficient of Variation and Fano Factor

Two key results link the Fano factor to fundamental properties of the spike train. If the spike train can be described by a renewal process, the distribution of spike counts will be approximatively normally distributed for large counting times T, with mean $N(T) \cong T/\bar{t}$ and variance $V(T) \cong \sigma_t^2 T/\bar{t}^3$. This is illustrated in figure 9.7B for the gamma distribution of order 2. While a normal distribution for $p(n)$ is expected from the law of large numbers, the formulas for $N(T)$ and $V(T)$ depend explicitly on the renewal nature of the spike train. Thus, for large T, we obtain (Cox 1962)

$$F(T) \cong \frac{\sigma_t^2 T}{\bar{t}^3}\frac{\bar{t}}{T} = C_V^2. \tag{9.17}$$

The relation between $F(T)$ and C_V can be explicitly verified in the case of the gamma distribution of order 2 (from eq. 9.16 and using the previously obtained value, $C_V = 1/\sqrt{2}$). This result motivates the following algorithm to verify whether the variability observed in a spike train is solely due to variability in the interspike intervals: (1) compute $F(T)$ as a function of T for a given experimental spike train; and (2) randomly reshuffle the interspike intervals of the experimental spike train to obtain a renewal process and compute $F_{shuffled}(T)$. If, for large T, the Fano factor $F(T)$ is different from $F_{shuffled}(T)$, variability in the spike count cannot be accounted for by variability in the interspike intervals alone. Furthermore, $F_{shuffled}(T)^{1/2}$ provides an estimate of C_V, by eq. 9.17. This algorithm has been applied to sensory neurons and has consistently led to the conclusion that a substantial portion of spike train variability is not explained by interspike interval variability (for a review, see Teich, Turcott, and Siegel 1996).

9.4.2 Relationship between Fano Factor and the Autocorrelation Function

Another result allows for a more precise understanding of the origin of variability observed in the spike count. For a *stationary* spike train (Cox and Lewis 1966), the index of dispersion is related to the correlation in spike occurrence times by the following formula (Cox and Isham 1980; Teich 1989):

$$F(T) = 1 + \frac{2}{f}\int_0^T d\tau \left(1 - \frac{\tau}{T}\right) R_{xx}^{+}(\tau). \tag{9.18}$$

In this equation, f is the mean firing rate and $R_{xx}^{+}(\tau)$ the autocorrelation function of the spike train for τ positive, a measure of the statistical dependency between two spikes as a function of the time interval τ separating them ($R_{xx}^{+}(\tau)$ is identical to the usual autocorrelation function except for a δ-function at the origin, which is removed; it is defined and discussed in section 9.6). For a Poisson process, $R_{xx}^{+}(\tau) = 0$, and we recover $F(T) = 1$ from eq. 9.18. In the case of a gamma distribution of order 2, we recover eq. 9.16 by plugging the results of eqs. 9.31 and 9.32 (section 9.6) into eq. 9.18. It follows in particular from this formula that if the correlation between spikes is only slowly decaying over time, $R_{xx}^{+}(\tau) \sim \tau^{-\alpha} (0 < \alpha < 1)$, for large τ, then

$$F(T) \sim T^{1-\alpha}, \tag{9.19}$$

for large T, or, equivalently,

$$V(T) \sim N(T)^{2-\alpha}, \tag{9.20}$$

using $N(T) = fT$. In other words, long range correlations in spike occurrence times implies a power law increase of $V(T)$ as a function of $N(T)$.

To detect such power law behavior, it is convenient to plot $(N(T), V(T))$ pairs for different values of T in log-log coordinates (Usher et al. 1994).[2] For a Poisson process, this procedures yields a line with unit slope. A more variable process will be revealed by a slope that is larger than one. In the limit of a slope equal to two ($\alpha = 0$ in the above equation), the fluctuations are so high as to cancel any beneficial effect obtained by averaging for longer times. In practice, neurons seldom show such power relationships over very large ranges of T. For instance, as emphasized previously, a refractory period has the effect of reducing variability for values of $T \approx t_{ref}$. Cells in visual cortex typically cluster on a one of slope between 1 and 1.4 over the relevant range of firing frequencies (Vogels, Spileers, and Orban 1989; Snowden, Treue, and Andersen 1992; Softky and Koch 1993).

9.5 Signal Detection and Receiver Operating Characteristic Analysis

Spike count distributions can also provide useful insights on the encoding of stimulus information by neurons, in addition to shedding light on the issue of variability considered in the last section. Changes in the mean firing rate as a function of stimulus parameters are usually the most conspicuous feature of neurons responses.

One way of assessing the information conveyed in the mean spike count is to optimally discriminate two stimuli on the basis of differences between the firing rates measured in an interval of length T. This paradigm, based on the concept of an ideal observer, has been applied to a wide range of sensory neurons and experimental stimuli. In retinal ganglion cells, the presence or absence of a dim light flash can be inferred with good accuracy from the mean firing rate observed in a 200 msec time window (Barlow, Levick, and Yoon 1971). Further examples include the discrimination of stimulus orientation from the responses of orientation selective neurons in area V1 of the macaque monkey (Vogels and Orban 1990) or of the direction of motion from neurons in cortical area MT (Newsome, Britten, and Movshon 1989; Britten et al. 1992). Here the performance of individual neurons, as assessed using the *ideal observer paradigm* discussed below, was comparable to the performance of the trained animal on the corresponding psychophysical task. This places constraints on how information from single cells is integrated across pools of neurons to give rise to the behavior of the animal.

Let us imagine a classical *yes-no rating experiment* (Green and Swets 1966), in which either one of two stimuli is presented, called stimuli 0 and 1. On each trial and

on the basis of an observation such as the mean spike count measured in an interval T, the subject has to decide which of stimuli 0 or 1 occurred. If the two stimuli result in different spike count distributions $p_0(n)$ and $p_1(n)$ being observed in an interval of duration T, an obvious strategy to determine the stimulus most likely to have caused a given spike count n_t is to compare the *likelihood ratio* $l(n) = p_1(n)/p_0(n)$ to a threshold criterion k and to choose stimulus 0 or 1 according to whether $l(n_t)$ is smaller or larger than threshold. The choice $k = 1$ corresponds to the inference[3]

$p_1(n_t) < p_0(n_t) \rightarrow$ stimulus 0,

$p_0(n_t) < p_1(n_t) \rightarrow$ stimulus 1.

The significance of values of k different from 1 will become clear as we proceed.

As a simple example, consider a Poisson neuron that fires at rates f_0 and f_1 ($f_0 < f_1$) in response to stimuli 0 and 1, respectively (Thibos, Levick, and Cohn 1979). From eq. 9.13

$$l(n) = \left(\frac{f_1}{f_0}\right)^n e^{-(f_1 - f_0)T}. \tag{9.21}$$

Two such Poisson spike count distributions and $l(n)$ are illustrated in figure 9.9A. The likelihood ratio of eq. 9.21 is a monotonic increasing function of n. In this case (the most common one), we can replace the criterion $l(n) \lessgtr k$ with the simpler rule

$n < k' \rightarrow$ stimulus 0,

$n > k' \rightarrow$ stimulus 1.

That is, if the observed spike count n is less than some threshold k', we infer that stimulus 0 was present; in the other case, we assume that stimulus 1 was present.

How good is this decision rule? Its performance can be precisely characterized by two quantities: (1) the *probability of false-alarm*, that is, the probability of concluding that stimulus 1 is present when in fact stimulus 0 occurred:

$$P_{FA} = \sum_{n \geq k'} p_0(n), \tag{9.22}$$

and (2) the *probability of correct detection*, that is, the probability of correctly concluding that stimulus 1 was present:

$$P_D = \sum_{n \geq k'} p_1(n). \tag{9.23}$$

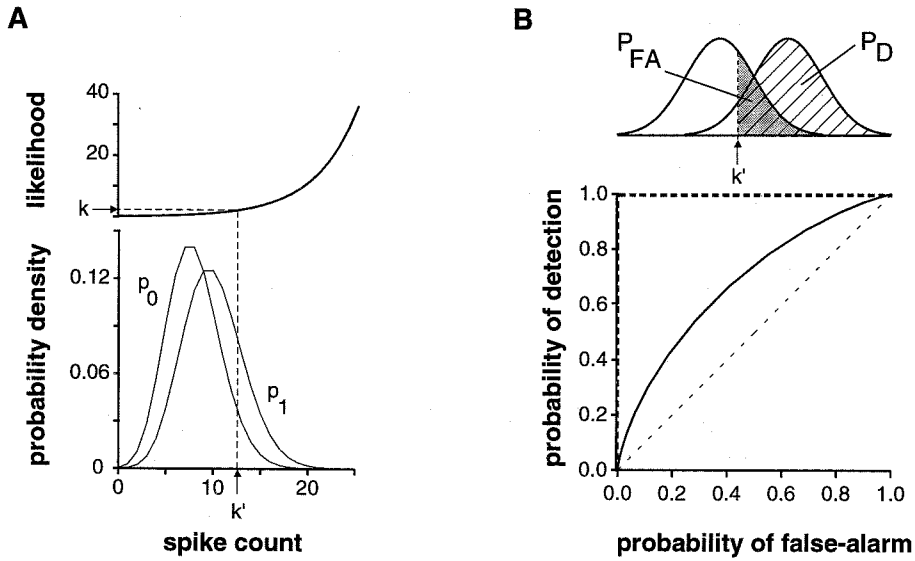

Figure 9.9
(A) Spike count distribution of a Poisson model with mean firing rates of 40 Hz and 50 Hz, respectively, corresponding to spike count densities p_0 (for stimulus 0) and p_1 (for stimulus 1; plotted for a $T = 200$ msec observation window). Likelihood ratio for these distributions shown on top. (B) ROC curve obtained by varying the threshold k' (see top illustration) from a very high value (in the limit of $k' \to \infty$, $P_D = P_{FA} = 0$) to a very low value (in the limit $k' \to -\infty$, $P_D = P_{FA} = 1$). For each value of the threshold k', the probability of false alarm P_{FA} (eq. 9.22; that is, believing that stimulus 1 was present while, in fact, stimulus 0 was present) is given by the integral of p_0 to the right of the threshold and is indicated by the gray surface (top illustration). The probability of detection P_D (eq. 9.23) of stimulus 1 corresponds to the integral of p_1 to the right of the threshold (hatched area). The ROC curve is a plot of this later area (P_D) as a function of P_{FA}. Dashed line below ROC curve: chance performance. On the opposite, the closer the ROC curve lies to the bold dashed lines, the better the performance.

It is clear from these equations that a fixed value of the threshold k' (or k) is equivalent to a fixed probability of false-alarm P_{FA} (or of correct detection P_D). Therefore, a plot of P_D as a function of P_{FA} completely characterizes the performance of the likelihood ratio test for all possible values of the threshold (see figure 9.9B). Such a plot is called the receiver operating characteristic of the likelihood ratio test or the ROC curve.[4] The diagonal line in figure 9.9B indicates chance performance ($P_{FA} = P_D$). The higher the ROC curve lies above the diagonal, the better the performance of the likelihood ratio test (the most favorable case being $P_D = 1$, independent of P_{FA}).

Remarkably, the likelihood ratio test is optimal: for a fixed probability of false-alarm P_{FA}, any alternative test used to decide between stimulus 0 and 1 from $p_0(n)$

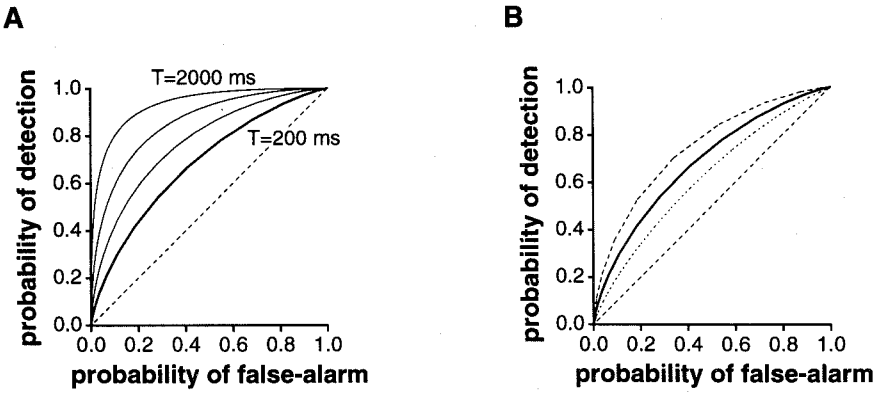

Figure 9.10
(A) ROC curves for the same model as in figure 9.9 and for increasing sampling times, $T = 200$ msec, $T = 500$ msec, $T = 1{,}000$ msec and $T = 2{,}000$ msec, respectively (only the two extreme curves are labeled). The performance of the ideal observer increases in parallel with the sampling time. In both panels A and B, the dashed straight line indicates chance level. (B) Middle curve (thick line) shows the discrimination performance of the ideal observer of two Poisson spike counts (same parameters as in figures 9.9B and 9.10A). The lower curve (dotted line) describes the performance of the ideal observer for spike counts distributed according to Neyman type-A (with same mean firing rates as in figure 9.9). The upper curve (dashed line) corresponds to the discrimination performance when the two spike counts are distributed according to gamma distributions of order 2 (see figure 9.7B).

and $p_1(n)$ will result in a smaller probability of detection P_D. In other words, any other test will yield an ROC curve below (or at best equal to) the ROC curve of the likelihood ratio test.[5] Note that because it remains unclear what type of decision rule nervous systems use, the optimal performance is the one obtained by an *ideal observer* who has complete access to the relevant probability distributions. Of course, the performance of the ideal observer will depend on properties of the spike trains and the interval chosen to measure the mean firing rate. In general, longer measuring intervals will lead to better performance by averaging out fluctuations, as illustrated for Poisson spike counts in figure 9.10A. Presently, the exact time interval over which neurons might average incoming information to perform a specific task is only weakly constrained. Similarly, spike trains that are more regular than Poisson ($C_V < 1$) will yield better discrimination performance, while spike trains with $C_V > 1$ will lead to worse performance (figure 9.10B).

As the measuring interval becomes large, the probability distribution of the spike count usually converges to a normal distribution by virtue of the law of large numbers (see section 9.4). In practice, the convergence can be quite fast, the Gaussian approximation being already accurate for spike counts as low as 10–20 (as in figure

9.7B). When the distributions $p_0(n)$ and $p_1(n)$ can be described by Gaussians of means and variances μ_i, σ_i (with $i = 0, 1$), respectively, the ROC curve can be computed exactly and is given by

$$P_D = 1 - \Phi\left(\frac{\sigma_0}{\sigma_1}\,\Phi^{-1}(1 - P_{FA}) - \frac{\mu_1 - \mu_0}{\sigma_1}\right), \tag{9.24}$$

where Φ is the cumulative probability distribution of a normalized Gaussian variable,

$$\Phi(x) = \frac{1}{\sqrt{2\pi}}\int_{-\infty}^{x} e^{-x^2/2}\,dx. \tag{9.25}$$

Values of $\Phi(x)$ are plotted in numerical tables or can be computed using well-known algorithms. Conversely, one can reexpress this equation in a different coordinate scale, $(\tilde{P}_{FA}, \tilde{P}_D)$, such that

$$P_{FA} = \Phi(\tilde{P}_{FA}), \quad P_D = \Phi(\tilde{P}_D). \tag{9.26}$$

This can be done using a simple command in MATLAB.

In this coordinate system, the ROC curve of eq. 9.24 corresponds to a straight line of slope $r = \sigma_0/\sigma_1$ and intercept $d' = (\mu_1 - \mu_0)/\sigma_1$ (Cohn, Green, and Tanner 1975). Changing coordinate scales is analogous to plotting exponential or power law functions on logarithmic paper, as illustrated in figure 9.11. In general, the larger the value of d', the easier the two distributions can be distinguished and the higher the performance.

When the standard deviations of the two spike count distributions are equal, $\sigma_1 = \sigma_0$, the ROC curve has unit slope and is completely characterized by the intercept d' commonly used in psychophysics (Green and Swets 1966). The value $d' = 1$ then corresponds to the two Gaussian distributions being separated by one standard deviation. However, usually for spike count distributions, the variance $V(T)$ is a function of the mean spike count $N(T)$, so that $\sigma_1 \neq \sigma_0$, and this special case is unlikely to occur.

9.6 Autocorrelation and Power Spectrum

While the mean spike count $N(T)$ is well suited to convey information about static components of a stimulus in a time interval of length T, stimulus parameters that vary over time during such an interval cannot be encoded by $N(T)$ alone. Modu-

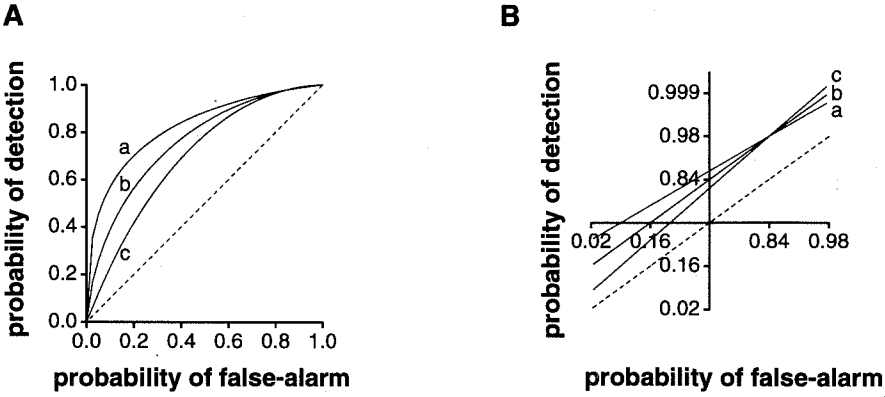

Figure 9.11
(A) Three ROC curves corresponding to the discrimination between two Gaussian distributions as the ratio of the two associated variances, $r = \sigma_0/\sigma_1$ and d' changes; d' is defined as the distance between the centers of the two Gaussians, normalized by σ_1. The parameters are: $r = 0.8$, $d' = 1.2$ for a, $r = 1$, $d' = 1$ for b and $r = 1.2$, $d' = 0.8$ for c. (B) On "normal" probability paper, corresponding to the change of coordinate of eq. 9.26, these curves are straight lines of slope r and intercept d' respectively (dashed line: chance level).

lation of the instantaneous firing rate around its mean value is an appropriate variable to encode such time-varying stimulus parameters.

Sections 9.6 and 9.7 survey a number of signal-processing techniques used to study stimulus encoding by means of instantaneous firing rate changes. In these techniques, the analysis of post stimulus time histograms (PSTHs) obtained from repeated presentations of a single stimulus is replaced by the analysis of average spike train properties in response to random stimulus ensembles. Such techniques represent a complementary approach to the more classical PSTH methods, shedding a different light on the encoding of time-varying stimuli in sensory neurons. By design, the techniques will work best if the neuronal system under study, whose input is the relevant stimulus parameter and whose output is the observed spike train, can be approximated by a linear, time-invariant (stationary) system. These assumptions are most likely to hold at early stages of sensory pathways (Wandell 1995; Rieke et al. 1996). Although further elaborations of these techniques can take into account nonlinearities and changes in the stimulus or neuron response over time, as explained below, none of them is expected to capture the encoding of stimulus parameters when the precise pattern of spikes is of importance, as is likely to be the case in the olfactory system of insects, for instance (Laurent 1996; Wehr and Laurent 1996).

While the instantaneous firing rate might convey information on a time-varying stimulus, it will also reflect intrinsic properties of the neurons themselves. In the

example of figure 9.3, fluctuations in instantaneous firing rate do not relate to the constant current input, but rather reflect different biophysical parameters (e.g., refractory period or passive time constant). We commence our investigation by characterizing how these properties affect the dynamics of neuronal firing.

9.6.1 The Autocorrelation Function

Second-order changes in the dynamics of neuronal firing are captured in the autocorrelation function of the spike train, which we now define. Let $x(t)$ be the spike train of a neuron, represented by a sequence of δ pulses at the time of spike occurrences $\{t_k\}$,

$$x(t) = \sum_k \delta(t - t_k). \tag{9.27}$$

It helps to visualize $x(t)$ as the instantaneous firing frequency of the neuron in a particular trial or observation period (with units of spk/sec; see chapter appendix A). The mean firing frequency is defined as the average over such an ensemble of observations, $m = \langle x(t) \rangle$ and is assumed to be independent of t (i.e., we assume that the spike train is stationary). Furthermore, a single—albeit very long—spike train of the ensemble is often assumed to be representative of the response of the system, so that ensemble averages can be replaced by time averages over the single sample. This is known as the "ergodicity assumption." To clarify this point, we show that under the ergodicity assumption, the mean firing rate f of a single neuron in a single trial is equal to the mean firing rate m (in spk/sec) averaged over the ensemble. Figure 9.12 illustrates the same point graphically. If N is the number of spikes in a large interval T, then

$$\begin{aligned} m &= \langle x(t) \rangle \\ &= \frac{1}{T} \int_0^T x(t)\, dt, \quad \text{for large } T \text{ (by ergodicity)}, \\ &= \frac{N}{T}, \end{aligned} \tag{9.28}$$

where $N/T = f$ is the mean firing rate for the representative sample spike train. (Similarly, other statistical properties of the ensemble can be computed by time averaging, as explained in chapter appendix A.) The autocorrelation function is defined as the average joint probability density of a spike at time t and $t + \tau$, minus their mean values,

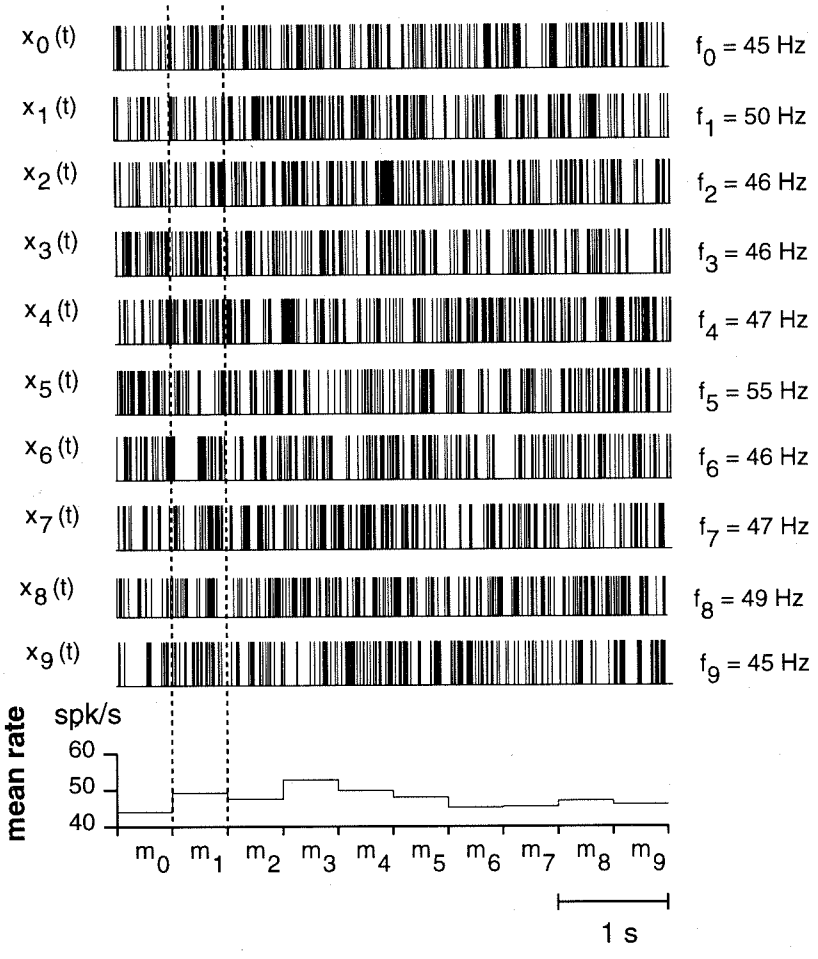

Figure 9.12
Traces labeled $x_0(t), \ldots, x_9(t)$ represent different spike trains of a Poisson neuron belonging to the same statistical ensemble which satisfies the assumptions of stationarity and ergodicity. They should be thought of as representing recordings from different nerve cells (assumed to be identical in their properties and response characteristics) or the response of a single cell to different realizations of a random stimulus. (Bottom) Mean firing rate m over 500 ms bins (m_0–m_9), obtained by averaging the firing rate of the ten samples (illustrated by two dashed lines for bin corresponding to m_1). Stationarity implies that m should be independent of the particular bin chosen: $m = m_0 = \cdots = m_9$ (i.e., a flat PSTH). Furthermore, m should be independent of the bin size (in the limit where the averaging is done over all spike trains of the ensemble). Ergodicity implies that the firing rate $f_0, \ldots, f_9$ for each single trace $x_0(t), \ldots, x_9(t)$ should be identical to m (in the limit where the recording time T is very long). Stationarity and ergodicity have analogous implications for higher order statistical functions, such as the autocorrelation.

$$R_{xx}(\tau) = \langle x(t)x(t+\tau)\rangle - m^2 \quad \text{(in units of (spk/sec)}^2\text{)}$$
$$= \langle (x(t)-m)(x(t+\tau)-m)\rangle. \tag{9.29}$$

Again, by time invariance (stationarity), $R_{xx}(\tau)$ is assumed to be independent of the absolute time point t. It follows from this assumption that $R_{xx}(\tau) = R_{xx}(-\tau)$. Subtracting m^2 enforces the normalization $R_{xx}(\tau) \to 0$, for large τ, because we expect two spikes to be uncorrelated for large time separations:

$$\langle x(t)x(t+\tau)\rangle = \langle x(t)\rangle\langle x(t+\tau)\rangle = m^2 \quad \text{(for } \tau \text{ large)}. \tag{9.30}$$

For a Poisson process, $R_{xx}(\tau) = m\delta(\tau)$. The δ-function at the origin corresponds to the sure event of a spike at point t given a spike at point t, while for $\tau \neq 0$ the autocorrelation function $R_{xx}(\tau)$ vanishes identically, meaning that two spikes separated by an arbitrary time interval τ are completely uncorrelated. This extreme case of eq. 9.30 is, of course, a consequence of the complete independence between two events which defines the Poisson process (see section 9.2.4). An alternative way of writing the autocorrelation function is

$$R_{xx}(\tau) = R^{+}_{xx}(\tau) + m\delta(\tau)$$
$$= m(m_x(|\tau|) - m) + m\delta(\tau), \tag{9.31}$$

where $m_x(\tau), \tau > 0$ is to be interpreted as the probability density of observing a spike at time $t+\tau$ when a spike occurred at time t. (Note that $m_x(\tau)$ is the probability density of observing *any* spike at time τ following a spike, not only the first one; Cox and Lewis 1966.) Thus values of $m_x < m$ (or, equivalently, $R^{+}_{xx}(\tau) < 0$) correspond to a suppressed probability of spiking as compared to the mean m, while values of $m_x > m$ (or $R^{+}_{xx}(\tau) > 0$) correspond to an increased probability of spiking. We illustrate these two possibilities in the following examples.

The interspike interval distribution of a gamma process of order 2 has a reduced probability of firing for short intervals when compared to a Poisson process (see figures 9.3A and 9.3B). Thus one expects a reduced probability of firing $m_x(\tau)$ or, equivalently, a negative correlation for small values of τ. In fact, $m_x(\tau)$ can be shown (Cox and Lewis 1966) to relax exponentially to its mean value $m = f = 1/\bar{t}$, with a time constant $\bar{t}/4$:

$$m_x(\tau) = m(1 - e^{-4\tau/\bar{t}}), \quad \tau > 0. \tag{9.32}$$

The two functions $m_x(\tau)$ and $R^{+}_{xx}(\tau)$ are plotted in figure 9.13A. Quite generally, the

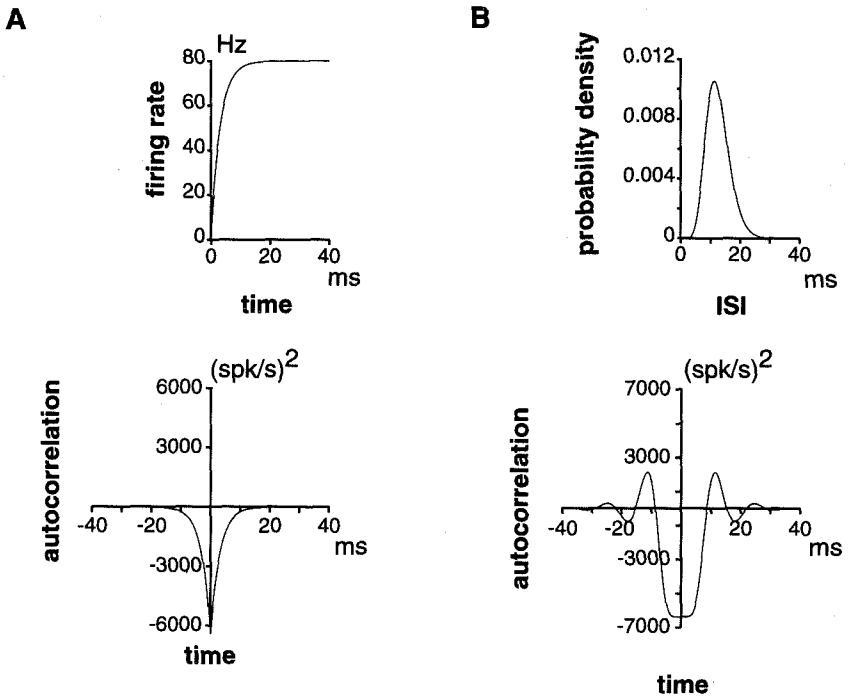

Figure 9.13
(A) Autocorrelation function R^{+}_{xx} (bottom graph) of a renewal gamma process of order 2. The mean firing rate of the model is 80 Hz. The negative correlation for short values of τ is due to the relative refractoriness of the model following a spike. The corresponding firing probability density function m_x (see eq. 9.32) is plotted on top. Its value is zero immediately after a spike, recovering exponentially toward steady state (80 Hz) with a time constant of 3.125 msec. (B) Autocorrelation function of a renewal gamma process of order 10 ($m = 80$ Hz, bottom graph). The positive peaks in the autocorrelation at ± 12.5 msec reflect the regularity of the ISI distribution (top graph) and coincides with the peak in the ISI distribution. In both panels A and B, the δ-function of R_{xx} at the origin has been subtracted, see eq. 9.31.

refractory period immediately following a spike will manifest itself by a negative correlation at short times τ.

Positive correlations can easily be observed in regular spike trains. This is illustrated in figure 9.13B for a gamma distribution of order 10 (see figure 9.3D). Such a model neuron has a very regular interspike interval distribution concentrated around its mean value, thus leading to positive correlations at multiples of the mean interspike interval.

9.6.2 The Power Spectrum

Because the autocorrelation function is real and symmetric (i.e., $R_{xx}(\tau) = R_{xx}(-\tau)$), its Fourier transform

$$S_{xx}(\omega) = \int_{-\infty}^{+\infty} R_{xx}(\tau) e^{i\omega\tau}\, d\tau \quad \text{(in units of (spk/sec)}^2\text{/Hz)}, \tag{9.33}$$

is also real and symmetric. In fact, $S_{xx}(\omega)$ is a positive function of frequency called the "power spectrum," which represents a measure of the frequency content of the spike train. The autocorrelation function can, of course, also be expressed in terms of the inverse Fourier transform, that is,

$$R_{xx}(\tau) = \frac{1}{2\pi} \int_{-\infty}^{+\infty} S_{xx}(\omega) e^{-i\omega\tau}\, d\omega. \tag{9.34}$$

For a Poisson process, the Fourier transform of $R_{xx}(\tau)$ yields $S_{xx}(\omega) = m$, and thus all frequencies are equally represented. As is clear from eq. 9.31, the power spectrum will usually contain additional terms, causing a departure from a flat spectrum when the spike train differs from Poisson. In the case of a gamma-distributed process of order 2 (see figure 9.3B), we obtain

$$S_{xx}(\omega) = m\left(1 - \frac{8m^2}{16m^2 + \omega^2}\right). \tag{9.35}$$

Thus the reduced probability of firing at short times τ (see eq. 9.32) causes a dip in the power spectrum at low frequencies, as illustrated in figure 9.14A. This is the usual manifestation of refractoriness in the frequency content of the spike train (Bair et al. 1994; Franklin and Bair 1995).

For regular spike trains, the peaks in the autocorrelation at multiple intervals of the mean interspike interval translate into peaks at the corresponding firing frequency and its harmonics, as illustrated in figure 9.14B for the gamma process of order 10.

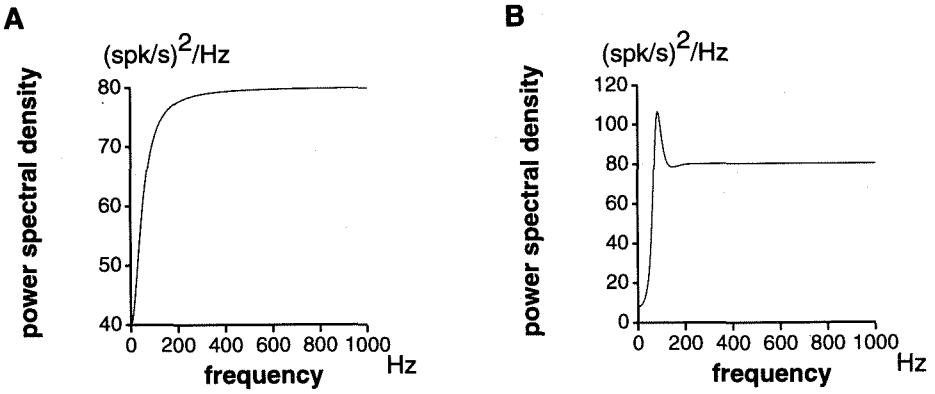

Figure 9.14
(A) Power spectrum of a renewal gamma process of order 2 (i.e., Fourier transform of the autocorrelation function of figure 9.13A). The negative correlation at short values of τ translates in a dip in the power spectral density at low frequencies. (B) For a renewal gamma process of order 10, the positive correlations at multiples of the mean ISI (see figure 9.13B) translate into a peak in power at the mean firing frequency (80 Hz).

9.6.3 Spike Train Analysis of Linear Encoding Systems

Let us now consider the response $x(t)$ of some neuronal system to an ensemble of stimuli $\{s_{mean} + s(t)\}$, where s_{mean} represents the mean stimulus (e.g., the mean luminance of a visual scene) and the ensemble $\{s(t)\}$ represents random variations around s_{mean}. We assume here that the entire system between the receptor and the neuron from which spikes are recorded can be described in the regime of interest, using a linear transfer function $K(t)$, and that the neuron encodes changes about s_{mean} by changes in its instantaneous firing rate. Using this knowledge, we would like to understand how the processing performed by the neuron on the stimulus will be reflected in the autocorrelation and power spectrum of the spike train.

We start by formulating our assumption precisely. Let $s_{mean} + s_0(t)$ be a representative stimulus drawn from the ensemble $\{s_{mean} + s(t)\}$ and let $f_{s_0}(t)$ be the changes in instantaneous firing rate,

$$f_{s_0}(t) = \langle x(t) - m \rangle_{(x|s_0)}, \tag{9.36}$$

averaged over many presentations of $s_{mean} + s_0(t)$. This average is denoted by $\langle \cdot \rangle_{(x|s_0)}$ to emphasize that $s_0(t)$ is fixed from one presentation to the next ($s_0(t)$ might be called "frozen noise"; figure 9.15). Our assumption is that changes in instantaneous firing rate are linearly related to $s_0(t)$ through a transfer function K,

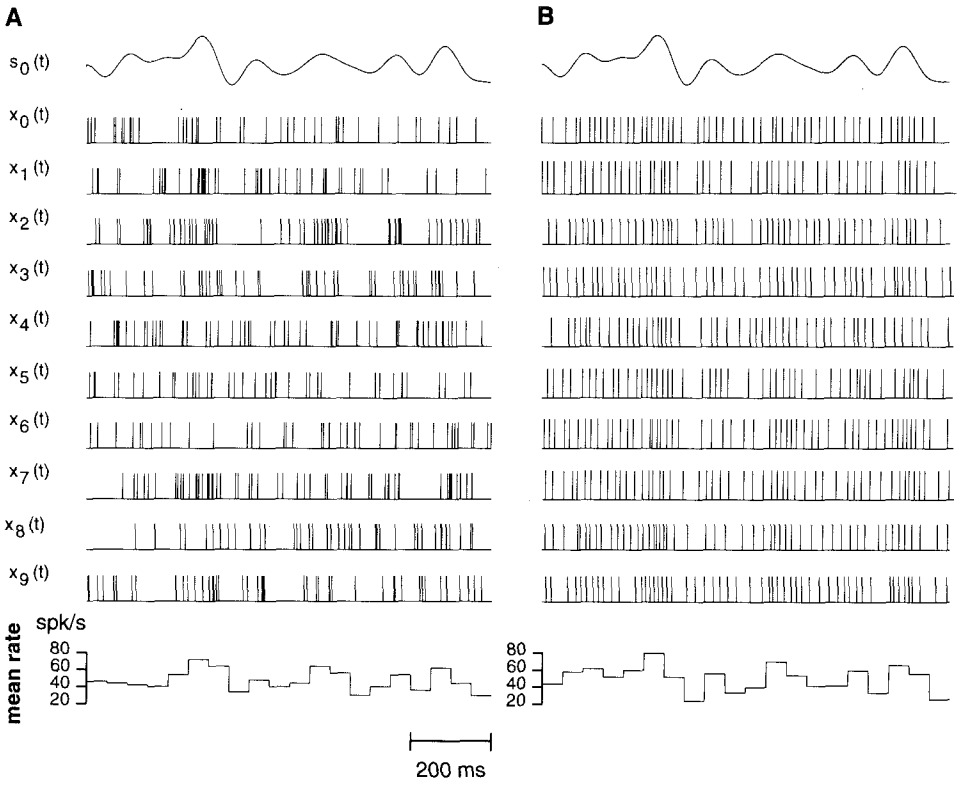

Figure 9.15
Ten spike trains of two different random threshold models in response to a single stimulus $s_0(t)$ (the "frozen noise" $s_0(t)$ is shown on top of both panels A and B). (A) Exponentially distributed threshold (corresponding to Poisson spike trains under constant inputs, figure 9.3A) leads to very irregular and varying spike trains from one presentation to the next. (B) Threshold of gamma order 10 (figure 9.3D) leads to much more regular and reproducible spike trains from one trial to the next. In spite of very different characteristics, both models encode the stimulus $s_0(t)$ in their instantaneous firing rate (see note 6), as may be seen by comparing the instantaneous firing rate (averaged over 50 msec) on the bottom of each panel to $s_0(t)$. The question of how reliably a single spike train from each one of these models encodes $s_0(t)$ will be addressed in section 9.7.3 (see figure 9.19).

$$f_{s_0}(t) = (K \star s_0)(t)$$
$$= \int_{-\infty}^{+\infty} dt_1 K(t - t_1) s_0(t_1), \tag{9.37}$$

where the symbol "$\star$" denotes convolution and where K has units of (spk/sec)/(unit stimulus/sec). This equation will hold exactly only if $(K \star s)(t) \geq -m$ (because the averaged instantaneous firing rate $m + f_{s_0}(t)$ cannot be negative), so that the effects of half-wave rectification can be neglected. To illustrate eqs. 9.36 and 9.37, consider again the random threshold models of figure 9.3 and let the constant current I be replaced by a time-varying current $i_{mean} + i_0(t)$. For each one of these models, the changes in instantaneous firing frequency averaged over many trials will be proportional to changes in the input current: $f_{i_0}(t) = \alpha i_0(t)$, with $\alpha = 1/C_m V_{th}$, so that our assumption is satisfied[6] (figure 9.15). Eq. 9.37 also holds when an arbitrary linear filter K is placed prior to the spike generation mechanism to mimic preprocessing of the stimulus before its encoding in output spike trains. An example of such a model whose mean instantaneous firing frequency reproduces the band-pass filtering properties of LGN relay cells is shown in figure 9.22.

It follows from eq. 9.37 that the correlations in instantaneous firing rate are related to correlations in the stimulus ensemble by

$$\langle f_s(t) f_s(t+\tau) \rangle_s = ((K \star \tilde{K}) \star R_{ss})(\tau), \tag{9.38}$$

where the average $\langle \cdot \rangle_s$ is over the stimulus ensemble, $R_{ss}(\tau)$ is the autocorrelation function of the stimulus, and $\tilde{K}(t) = K(-t)$. Furthermore, let us assume that correlations in the occurrence of single spikes are dominated by correlations in the stimulus

$$\langle (x(t) - m)(x(t+\tau) - m) \rangle_{(x|s_0)} = \langle x(t) - m \rangle_{(x|s_0)} \langle x(t+\tau) - m \rangle_{(x|s_0)}, \tag{9.39}$$

for $\tau \neq 0$, so that effects like those of refractoriness or regularity considered above can be neglected.[7] In the case of a leaky integrator, we expect this condition to require that the correlations in the stimulus should occur on a much longer time scale than τ_m. By taking averages over the stimulus ensemble on both sides of eq. 9.39, we obtain

$$R^+_{xx}(\tau) = \langle f_s(t) f_s(t+\tau) \rangle_s. \tag{9.40}$$

Combining eqs. 9.31, 9.38, 9.40 and Fourier-transforming results in

$$S_{xx}(\omega) = |K(\omega)|^2 S_{ss}(\omega) + m, \tag{9.41}$$

where the additive factor m originates from the δ-function at the origin in eq. 9.31. A

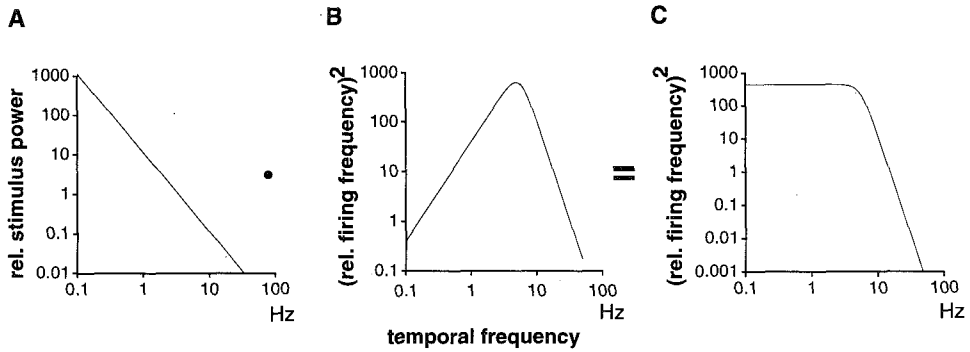

Figure 9.16
Graphical illustration of eq. 9.41 for natural visual stimuli and their processing by relay cells in the cat lateral geniculate nucleus (LGN) in normalized units. (A) Power spectral density of natural visual scenes has a temporal power spectrum that decays quadratically in frequency. (B) Transfer function of LGN relay cells is band-pass in the temporal domain. (C) Multiplication of the functions in panels A and B yields an output spike train spectrum (the constant value m has been subtracted) that is flat in temporal frequency, thus effectively decorrelating the visual input signal. It has been argued by Dong and Atick (1995) that one function of the LGN is to decorrelate the visual input signal, giving rise to a more effective and less redundant representation of visual stimuli in cortex proper.

different derivation of this equation under the assumption of complete half-wave rectification can be found in Gabbiani and Koch 1996 and Gabbiani 1996.

Equation 9.41 states that the power spectrum of the spike train will be related to the power spectrum of the stimulus by multiplication with the square modulus of the frequency response of K. One way to determine the transfer function K is to apply the Wiener kernel method, described in section 9.7.

We consider one example illustrating possible applications of eq. 9.41. The response of relay cells in the lateral geniculate nucleus to sinusoidal gratings of varying temporal frequencies can be used to determine their linear transfer characteristics. In the frequency domain, the energy of the corresponding filter, $|K(\omega)|^2$, is band-pass as illustrated in figure 9.16B (Saul and Humphrey 1990). Measurements of the temporal power spectrum of natural images, $S_{ss}(\omega)$, show that it decays according to a power law with temporal frequency (see figure 9.16A; Dong 1995). Therefore, multiplying $|K(\omega)|^2$ with $S_{ss}(\omega)$ predicts that the power spectrum of LGN spike trains in response to natural stimuli should be flat in frequency up to 10 Hz (see figure 9.16C; Dong and Atick 1995). This encoding of temporal changes in natural images by LGN spike trains is optimal because it amplifies the frequencies that are less well represented in the stimulus, thus whitening the input. This prediction obtained from $S_{ss}(\omega)$, $|K(\omega)|^2$ and eq. 9.41 for the encoding of natural stimuli in spike trains of LGN relay cells has been confirmed experimentally (Dan, Atick, and Reid 1996).

9.7 Wiener Kernels and Stimulus Estimation

Starting from the assumption of linear encoding formulated in section 9.6.3, we now explain how the transfer function characterizing the processing performed by a neuron can be computed. This is a *forward problem*, which has been extensively investigated both theoretically and experimentally. For a particular choice of the random stimulus ensemble, it is equivalent to the computation of the first-order Wiener kernel, as explained below. Next, we address the problem of how accurately a time-varying stimulus can be encoded in a single spike train. This problem is for time-varying stimuli what the problem considered in section 9.5 is for static stimuli: how accurately can single neurons convey information in their mean spike count? To solve it, we must solve the corresponding *inverse problem*, that is, we must determine how accurately a time-varying stimulus can be estimated from a single-spike train. This problem has been addressed experimentally in the fly visual system (Bialek et al. 1991), in the electrosensory system of weakly electric fish (Wessel, Koch, and Gabbiani 1996), and in the cercal system of the cricket (Theunissen et al. 1996; Roddey and Jacobs 1996). Finally, we also investigate to what extent the linear assumption of section 9.6.3 is altered by nonlinearities in the encoding.

9.7.1 First-Order Wiener Kernel and Reverse Correlation

The problem of estimating the transfer function K introduced in eq. 9.37,

$$f_{s_0}(t) = \langle x(t) - m \rangle_{(x|s_0)} = (K \star s_0)(t), \tag{9.42}$$

can be solved by correlating $s(t)$ with $x(t)$. We define the *cross-correlation* between the stimulus and spike train by

$$\begin{aligned} R_{sx}(\tau) &= \langle s(t)(x(t+\tau) - m) \rangle \\ &= \langle s(t)x(t+\tau) \rangle, \end{aligned} \tag{9.43}$$

where the second equality follows from the normalization $\langle s(t) \rangle = 0$ introduced in section 9.6.3. The cross-correlation $R_{sx}(\tau)$ is related to the autocorrelation of the stimulus through

$$R_{sx}(\tau) = (K \star R_{ss})(\tau), \tag{9.44}$$

using eq. 9.42. If we let $S_{sx}(\omega)$ denote the Fourier transform of $R_{sx}(\tau)$, we obtain $S_{sx}(\omega) = K(\omega)S_{ss}(\omega)$ after Fourier-transforming both sides of eq. 9.44. Therefore, the frequency response of K is given by

$$K(\omega) = \frac{S_{sx}(\omega)}{S_{ss}(\omega)}. \tag{9.45}$$

The computation of K is further simplified if the random stimuli $s(t)$ are chosen to have a power spectrum constant with frequency $S_{ss}(\omega) = \sigma^2$, corresponding to a *white* or uncorrelated stimulus, $R_{ss}(\tau) = \sigma^2\delta(\tau)$ (in practice, the stimulus is chosen to be white until a cutoff frequency above the one of the system under study). Plugging the value of $S_{ss}(\omega)$ into eq. 9.45 and Fourier-transforming back to the time domain yields $K(\tau) = (1/\sigma^2)R_{sx}(\tau)$. By using eq. 9.43, the representation $x(t) = \sum_{k=1}^{N} \delta(t - t_k)$, where N is the number of recorded action potentials and $f = N/T$ the mean firing rate, we obtain

$$K(\tau) = \frac{f}{\sigma^2}\frac{1}{N}\left(\sum_{k=1}^{N} s(t_k - \tau)\right). \tag{9.46}$$

This is the celebrated *reverse-correlation formula* for K, stating that the linear transfer function of the neuron can be recovered by a simple spike-triggered average of the stimulus preceding the spikes (de Boer 1973). This technique has been applied to many different neurons at various early stages of sensory systems, for example, in cat and monkey striate visual cortex (McLean and Palmer 1989; DeAngelis, Ohzawa, and Freeman 1993; Reid and Alonso 1995). An example illustrating the computation of K from eq. 9.45 is shown in figure 9.17 for the LGN relay cell model depicted in figure 9.22.

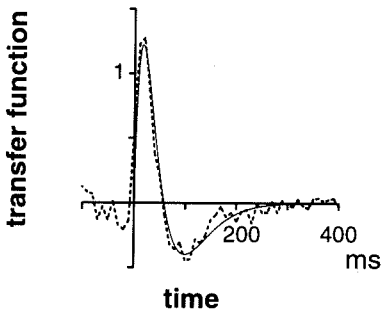

Figure 9.17
Computation of a linear transfer function using the Wiener kernel method. The solid line represents the transfer function of the model shown in the central panel of figure 9.22. The dotted line represents the estimate obtained from eq. 9.45, by cross-correlating the stimulus (shown in the right lower panel of figure 9.22 with the output spike train of the neuron (lower left panel of figure 9.22. The left axis has dimension of (spk/sec)/(unit stimulus) and has been normalized.

9.7.2 Nonlinear Encoding and Higher Kernels

If the relation between stimulus changes and instantaneous firing frequency changes is nonlinear, a transfer function $W_1(\omega)$ can still be obtained experimentally using either eq. 9.45 or 9.46, but the question of its relation to stimulus encoding by the neuron is now raised. We illustrate the significance of $W_1(\omega)$ in such cases by the following observations.

First, let us assume that the relation between stimulus and instantaneous firing frequency changes is obtained by passing $y(t) = (K \star s)(t)$ through a nonlinear function $g(y)$,

$$f_{s_0}(t) = g(y(t)), \quad y(t) = (K \star s)(t), \tag{9.47}$$

implementing half-wave rectification, compression or saturation, for instance (such a sigmoid nonlinearity is illustrated in figure 9.21A). The function g is called a "static or memoryless nonlinearity" because the output $f_{s_0}(t)$ depends only on y at time t. Because of the convolution operation with K, however, $f_{s_0}(t)$ will depend on past values of the stimulus. Let us now assume that the stimulus ensemble is *Gaussian*. By definition, this means that for arbitrary times, $t_1, \ldots, t_n$ the stimulus vector $(s(t_1), \ldots, s(t_n))$ is a jointly Gaussian random vector. This property must hold for *all* values of $n = 1, 2, 3, \ldots$.[8] Under this assumption, the cross-correlation between the stimulus and spike train can still be computed exactly:

$$R_{sx}(\tau) = c(K \star R_{ss})(\tau), \quad c = \frac{\langle yg(y) \rangle}{\sigma_y^2}, \tag{9.48}$$

where σ_y^2 is the variance of $y(t) = (K \star s)(t)$. This result is known as "Bussgang's theorem" (Bendat 1990). For example, if $y(t)$ is considered to be the somatic current driving the cell, then Bussgang's theorem states that it is possible to recover the cross-correlation between the stimulus and the somatic current from the cross-correlation between the stimulus and the output spike train (under the assumption of eq. 9.47). Up to a constant factor c, the cross-correlation of eq. 9.48 is identical to the one obtained in the linear case (eq. 9.44). Thus the effects of a static nonlinerity are *not* reflected in the time course of $W_1(\tau)$, but its presence can nevertheless be detected by using input stimuli with different variances (because c depends on the variance of the stimulus).

In the nonlinear case, the significance of $W_1(\tau)$ can be understood by considering the following question. In response to the stimulus $s(t)$, which linear function $(h \star s)(t)$ best approximates the instantaneous firing rate of the neuron in the sense that the mean square error,

$$\varepsilon^2(h) = \langle [(h \star s)(t) - f_s(t)]^2 \rangle_s, \tag{9.49}$$

is minimized when averaged over the stimulus ensemble? This equation can be solved by using the fact that at the minimum, the first-order derivative $d\varepsilon^2/dh$ has to vanish. Solving for h yields $h(\tau) = W_1(\tau)$. Thus the transfer function $W_1(\tau)$ is the best *linear estimator* for the response of the cell (in the mean square sense). The accuracy of this estimate will depend to a large extent on the nature of the nonlinearity and can fail completely in certain cases.[9]

In principle, it can be improved by considering estimators consisting of higher-order functions of the stimulus

$$g_s(\tau) = \mathbf{W_1}(s(t))(\tau) + \mathbf{W_2}(s(t_1), s(t_2))(\tau) + \cdots, \tag{9.50}$$

where $\mathbf{W_1}(s(t))(\tau) = (W_1 \star s)(\tau)$, and so on. When the stimulus ensemble used is Gaussian white noise, the functionals $\mathbf{W_n}$ are called "nth-order Wiener kernels" and procedures are known to compute them,[10] although these nonlinear methods lack the simplicity and generality of the linear case (Palm and Poggio 1977). It is, for example, unclear how the results obtained with one stimulus ensemble will generalize to other stimuli. Even for simple static nonlinearities as half-wave rectification, an infinite number of terms is needed in the series of eq. 9.50. In some cases, considerable progress has been made by combining such methods with specific assumptions on the type of nonlinearities involved (Victor 1987, 1988; Sakai, Naka, and Korenberg 1988).

9.7.3 Stimulus Estimation and Reliability of Encoding

While the first-order Wiener kernel method fully characterizes the linear encoding of time-varying stimuli by instantaneous firing rate changes, it has some shortcomings. Because it focuses on predicting the ensemble average response to the stimulus, the first-order Wiener kernel does not, for example, directly assess how much information about a time-varying stimulus is contained in a single spike train. All the models illustrated in figure 9.3 are able to encode stimulus changes by instantaneous firing rate changes (see note 6), but clearly the information contained in single spike trains will depend on the noise corrupting the encoding. In these examples, it can range from extreme (in the Poisson case) to noise-free (in the integrate-and-fire model; see figure 9.15).

The problem of how reliably a single spike train encodes a time-varying stimulus can be successfully addressed by estimating the stimulus from the spike train and characterizing the accuracy of the estimate. Such an estimate can be obtained by *Wiener-Kolmogorov filtering*, a signal-processing technique complementary to first-

order Wiener kernel analysis and closely related to it (Poor 1994). We consider again a neuron encoding a stimulus by changes in its instantaneous firing rate:

$$f_s(t) = \langle x(t) - m \rangle_{(x|s)} = (K \star s)(t). \tag{9.51}$$

If we let $x_0(t)$ denote the spike train with its mean firing rate subtracted, $x_0(t) = x(t) - m$, then a linear estimate of the stimulus given the spike train can be obtained by convolving $x_0(t)$ with a filter $h(t)$, $s_{est}(t) = (h \star x_0)(t)$. Because of the discrete nature of the spike train, this amounts (up to a constant factor) to placing a copy of h around each spike,

$$s_{est}(t) = \sum_{k=1}^{N} h(t - t_k) - m \int_{-\infty}^{+\infty} h(t)\, dt, \tag{9.52}$$

to estimate deviations $s(t)$ of the stimulus from its mean value. The filter h is chosen to minimize the mean square error between the stimulus and its estimate,

$$\varepsilon^2(h) = \langle [s(t) - h \star x_0(t)]^2 \rangle, \tag{9.53}$$

and is thus the optimal linear estimator given the spike train (in the mean square sense). Eq. 9.53 is solved in the same way as eq. 9.49. Imposing the condition $d\varepsilon^2/dh = 0$ for the optimal filter and solving for h yields

$$h(\omega) = \frac{S_{sx}(-\omega)}{S_{xx}(\omega)}. \tag{9.54}$$

This formula is almost identical to the formula for $W_1(\omega)$, with $S_{xx}(\omega)$ playing the role of $S_{ss}(\omega)$. In particular, if the power spectrum of the spike train is flat, $S_{xx}(\omega) = m$ (i.e., Poisson), then $h(\omega) = (1/m)S_{sx}(-\omega)$, from which it follows that $h(\tau) = (1/m)R_{sx}(-\tau)$ is also determined by a simple spike-triggered average. This condition is usually satisfied at low firing rates, when spikes can be considered as nearly independent of each other (Gabbiani and Koch 1996; Wessel, Koch, and Gabbiani 1996). In general, the filter h computed from eq. 9.54 will not be causal in the sense that $h(t) \neq 0$ for $t > 0$, meaning that the occurrence of a spike can be used to predict the future time course of the stimulus (possible only because of the presence of correlations in the stimulus and of the response properties of the neuron). Therefore, the filter h represents a *noncausal ideal linear observer* of the spike train in the sense of section 9.5. Causal (ideal) observers and nonlinear (ideal) observers have been described in the literature (Snyder 1975; Bialek et al. 1991; Poor 1994).

If no correlations exist between $s(t)$ and $x(t)$ (i.e., $S_{sx}(\omega) = 0$ for all frequencies ω), the best linear estimator of $s(t)$ is equal to the mean value, $\langle s(t) \rangle = 0$. The

maximal mean square error computed from eq. 9.53 is then equal to the variance of the stimulus, $\varepsilon^2_{max} = \sigma^2_s$. It is therefore convenient to quantify the accuracy of stimulus encoding by normalizing the root mean square error computed from $s(t)$, $x_0(t)$, and eqs. 53–54 by its maximal value σ_s,

$$\varepsilon_r = \frac{\sqrt{\varepsilon^2}}{\sigma_s}, \tag{9.55}$$

so that ε_r takes values between 0 and 1, with $\varepsilon_r = 0$ corresponding to perfect estimation and $\varepsilon_r = 1$ to an estimation performance not better than chance level. Equivalently, the *coding fraction*, $\gamma = 1 - \varepsilon_r$, represents the percentage of temporal stimulus fluctuations encoded, in units of the stimulus standard deviation.

The performance of stimulus encoding as a function of frequency is characterized by computing the *noise* in the stimulus estimate,

$$n(t) = s(t) - s_{est}(t), \tag{9.56}$$

and comparing the relative power of the noise and stimulus,

$$SNR(\omega) = \frac{S_{ss}(\omega)}{S_{nn}(\omega)}. \tag{9.57}$$

This signal-to-noise ratio is equal to 1 when estimation is at chance level for a given frequency (i.e., when there is as much noise as there is signal power at that frequency) and tends to infinity for perfect estimation.[11]

An example of stimulus estimation from the spike train of a Poisson model encoding a time-varying random current $i_{mean} + i_0(t)$ is shown in figure 9.18. When the correlations in single-spike occurrences are dominated by correlations in the stimulus (this condition is exactly satisfied in the Poisson model; see note 7), the power spectrum of the spike train is given by eq. 9.41 so that the linear estimation filter can be computed exactly from knowledge of the linear system's transfer function K:

$$h(\omega) = \frac{K(-\omega)S_{ss}(\omega)}{m + |K(\omega)|^2 S_{ss}(\omega)}, \tag{9.58}$$

using eqs. 9.45 and 9.54. A number of observations can be made using this result (Gabbiani and Koch 1996; Gabbiani 1996). In particular, for a fixed mean firing rate m, the fraction of the stimulus encoded, γ, will increase with the standard deviation of the stimulus σ_s (or its contrast, σ_s/s_{mean}). This is because larger values of σ_s correspond to larger fluctuations in the instantaneous firing rate $\sigma_f = \langle x_0(t)^2 \rangle$ (see eq.

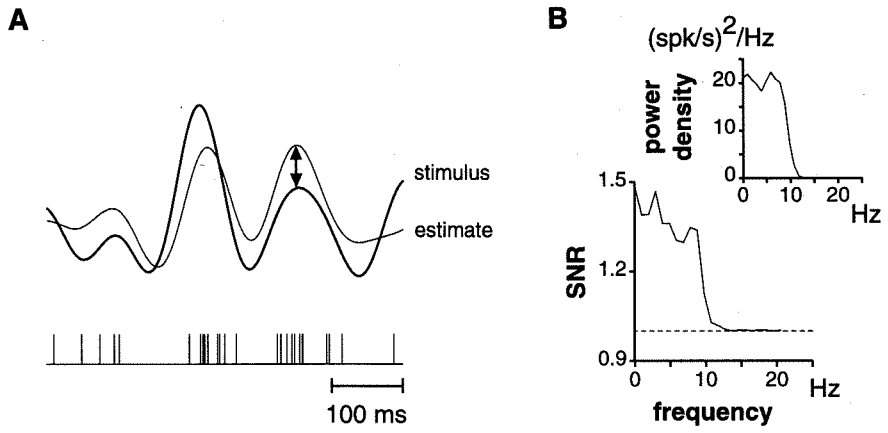

Figure 9.18
Stimulus estimation for a Poisson neuron firing at a mean rate of 50 Hz. (A) Instantaneous firing frequency of the neuron model is proportional to the stimulus (i.e., in this example, there is no filtering by the neuron model, $K(t) = \delta(t)$). In turn, the stimulus is estimated from the spike train (shown at the bottom) by placing the optimal linear filter computed from eq. 9.54 around each spike, as explained in eq. 9.52. To compute the mean square error, the difference between stimulus (thick line) and estimate (thin line) at each time point (illustrated by the double arrow) is computed and squared; the average is then taken over all time points of the observation (see eq. 9.55). Here the fraction of the stimulus encoded is only $\gamma = 0.14$. (B) Signal-to-noise ratio (SNR) for the estimation, indicating the performance of the neuron as a function of frequency (eq. 9.57). The dashed line ($SNR = 1$) indicates chance level. If we compare the SNR curve with the frequency content of the stimulus (upper graph), we see that all frequencies are equally well encoded.

9.51), which encode the stimulus more reliably. For a fixed firing rate *contrast*, σ_f/m, the fraction of the signal encoded will increase with the mean firing rate, m. This can be explained by an increased sampling of the stimulus in the spike train. Finally, the accuracy of stimulus encoding will depend on the characteristics of the stimulus. If, for instance, the frequency content of the stimulus used is not matched to the processing characteristics of the recorded cell (i.e., if there is a substantial range of frequencies for which the signal-to-noise ratio is equal to 1), then the accuracy of stimulus encoding will decrease. In such cases, it is meaningful to estimate only the range of frequencies encoded by the cell, by filtering out from the stimulus frequencies for which $SNR = 1$. The presence of such frequencies will depend on the stimulus used (through $S_{ss}(\omega)$) and the processing performed by the cell (through $K(\omega)$). Similarly, stimuli with natural statistics are expected to yield higher values of the coding fraction because they are more predictable than Gaussian stimuli.

Figure 9.19 illustrates the effect of encoding noise on the accuracy of stimulus estimation from single-spike trains. A white stimulus $s(t)$ with a cutoff frequency of

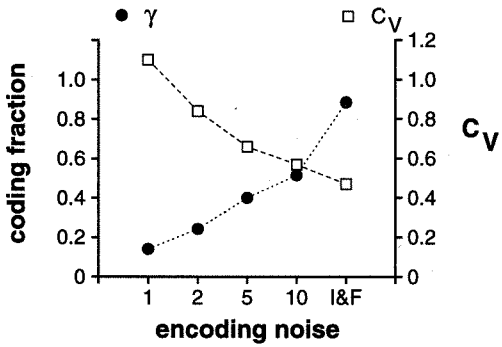

Figure 9.19
Fraction γ of the white stimulus (10 Hz cutoff frequency) shown in figures 9.18 and 9.20 that can be recovered from single-spike trains of various neuron models (mean firing rate: 50 Hz). The bottom axis shows the order of the threshold gamma distribution implementing encoding noise. These models are identical to those of figure 9.3 (except that the refractory period has been set to zero). While a Poisson neuron ($n = 1$) encodes relatively poorly the stimulus ($\gamma = 14\%$), a single perfect integrate-and-fire neuron is quite accurate ($\gamma = 88\%$).

10 Hz (figures 9.18B and 9.15) was estimated from the spike trains of the different models illustrated in figure 9.3. Examples of a single stimulus from this ensemble and the responses of two models are shown in figure 9.15. The fraction of the stimulus encoded is plotted for each one of these models in figure 9.19. A single spike train of a Poisson neuron (figure 9.15A) is able to encode $\gamma = 14\%$ of the stimulus, implying that to obtain an estimate to $\gamma = 90\%$ accuracy, an average of over $N = 74$ independent spike trains is needed (by the usual $\sqrt{N}$ argument; Shadlen and Newsome 1994; Gabbiani 1996). In contrast, an integrate-and-fire neuron firing at the same rate will encode $\gamma = 88\%$ of the stimulus, so that only $N = 2$ independent spike trains will yield an estimate with a better accuracy. Plotted on the same figure is the C_V of the spike trains used to estimate γ. The C_V goes down as stimulus estimation improves because in these models additional noise in the encoding translates into a larger variability of the spiking output. Even in the case of a perfect integrator, however the $C_V = 0.47$ amounts to half that of a Poisson spike train. This variability is not due to noise but is fully devoted to encoding the stimulus in the interspike intervals of the model spike trains. The theoretical numbers illustrated in figure 9.19 are indicative of how many neurons are needed to encode accurately a time-varying stimulus; single and multiple simultaneous recordings that take into account correlations between nerve cells are expected to settle these questions experimentally.

9.7.4 More General Estimation Techniques

It is worth emphasizing that the optimal linear filter $h(\tau)$ depends only on the cross-correlation $R_{sx}(\tau)$ and the autocorrelation $R_{xx}(\tau)$, as this has important implications. For example, one might be surprised to obtain a good estimate of $s(t)$ with the filter of eq. 9.54 because the Wiener-Kolmogorov filtering technique was originally designed to deal with a completely different situation: the recovery of $s(t)$ from continuous observations buried in Gaussian white noise. As is clear from eq. 9.54, however, any other random observation $r(t)$ that has the same cross-correlation $R_{sr}(\tau) = R_{sx}(\tau)$ with the stimulus and autocorrelation function $R_{rr}(\tau) = R_{xx}(\tau)$ as the spike train $x(t)$ will lead to exactly the same estimation problem. This will be so even if $r(t)$ is strikingly different from $x(t)$. Consider the case of a Poisson model, as in the previous paragraph. It is easy to see that if, instead of observing the spike train, we observed

$$r(t) = (K \star s)(t) + m^{1/2} w(t), \tag{9.59}$$

where $w(t)$ is Gaussian white noise with unit variance, $R_{ww}(\tau) = \delta(\tau)$, then we would be led to the same estimation filter of eq. 9.54 and the same performance (Snyder 1975). Thus, in this case, estimation from the spike train is *equivalent* to estimation from an observation of $(K \star s)(t)$ buried in Gaussian white noise. The difference between the two signals $x(t)$ and $r(t)$ is illustrated in figure 9.20. This remark is important because it implies that improved estimation techniques developed for the additive Gaussian case can also be expected to work when applied to neuronal spike trains. These techniques include adaptive filtering, where the shape of the filter $h(\tau)$ is time-dependent to take into account firing rate adaptation, changes in the mean stimulus value, or contrast level over time. In addition, nonlinear techniques have been applied successfully to certain types of stimuli. (For examples illustrating these techniques and for further references, see Snyder 1975, chapter 6.)

9.7.5 Nonlinear Encoding and Stimulus Estimation

If the relation between stimulus changes and instantaneous firing rate changes is nonlinear, the accuracy of stimulus estimation will again depend to a large extent on the type of nonlinearity involved. A neuron that encodes specific features of a time-varying stimulus and disregards most of its time course (such as might be implemented by a static threshold nonlinearity) will yield poor estimation results (Gabbiani et al. 1996; Sheinberg and Logothetis 1997). By contrast, other nonlinearities like firing rate saturation and half-wave rectification are not expected to alter significantly

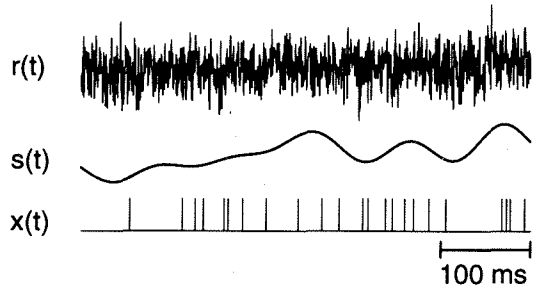

Figure 9.20
Stimulus $s(t)$ shown in the middle (thick line) can be estimated from the spike train of a Poisson neuron $x(t)$ (bottom trace, as in figure 9.18) or from the noisy continuous observation shown on top, $r(t)$. While these two estimation problems appear very different, they are in fact completely identical because the autocorrelations and cross-correlations of both observations with the stimulus are the same. As the top trace makes clear, this estimation problem is a difficult one. The fraction of the signal recovered from the noisy observation or from the spike train by linear estimation is 14% (see figure 9.18).

stimulus estimation results (Wessel, Koch, and Gabbiani 1996). Certain types of nonlinearities will even improve the encoding of time-varying stimuli in single spike trains under adequate conditions. To illustrate this point, we consider again encoding through a static nonlinearity as in eq. 9.47 and spike trains for which eq. 9.39 holds, so that the power spectrum can be computed exactly (see eq. 9.41).

Deviation from linear encoding can be assessed by computing the *magnitude coherence* between the stimulus and instantaneous firing rate,

$$|C_{sf_s}(\omega)| = \frac{|S_{sf_s}(\omega)|}{S_{ss}(\omega)^{1/2} S_{f_s f_s}(\omega)^{1/2}}, \tag{9.60}$$

where $S_{sf_s}(\omega) = S_{sx}(\omega)$ is the Fourier transform of the cross-correlation between stimulus and instantaneous firing frequency, while $S_{f_s f_s}(\omega)$ is the power spectrum of the instantaneous firing rate. The magnitude coherence is a frequency-dependent correlation coefficient measuring the extent of the linear relation between s and f_s (Carter 1987; Ljung 1987). For each frequency ω_0, $|C_{sf_s}(\omega_0)|$ takes values between 0 and 1. If $|C_{sf_s}(\omega_0)| = 0$, the relation between s and f_s is not linear (or nonexistent, $S_{sf_s}(\omega) = 0$). when $|C_{sf_s}(\omega_0)| = 1$, the stimulus s and the instantaneous firing rate f_s are perfectly linearly correlated. In the case where f_s is determined by s through eq. 9.42, it follows from eqs. 9.38 and 9.45 that $|C_{sf_s}(\omega_0)| = 1$ at all stimulus frequencies. From eq. 9.41, we know that $S_{xx}(\omega) = S_{f_s f_s}(\omega) + m > S_{f_s f_s}(\omega)$. Thus the magnitude coherence between the stimulus and spike train,

$$|C_{sx}(\omega)| = \frac{|S_{sx}(\omega)|}{S_{ss}(\omega)^{1/2} S_{xx}(\omega)^{1/2}}$$
$$= \left(\frac{SNR(\omega) - 1}{SNR(\omega)}\right)^{1/2}, \tag{9.61}$$

yields a conservative estimate of linearity between stimulus and instantaneous firing rate, $|C_{sf_s}(\omega)| \geq |C_{sx}(\omega)|$. Experimental values of $|C_{sx}(\omega)|^2$ have been reported for wind-sensitive sensory neurons in the cricket cercal system (Theunissen et al. 1996; Roddey and Jacobs 1996). While $|C_{sx}(\omega)|$ does not directly measure the linearity of stimulus encoding, it has the advantage of being directly related to the performance of stimulus estimation through eq. 9.61. This equation can be derived from the definition of the noise, $n(t)$, and of the signal-to-noise ratio, $SNR(\omega)$ (see eq. 9.57; Gabbiani 1996; Theunissen et al. 1996). In contrast, $|C_{sf_s}(\omega)|$ is not in general related to stimulus estimation performance from single-spike trains,[12] as explained below.

To illustrate the behavior of these two functions in a nonlinear situation, we return to the example of a Poisson neuron firing at a mean rate of 50 Hz and encoding a Gaussian random stimulus with a cutoff frequency of 10 Hz in its instantaneous firing rate, as in figure 9.18. This input modulates the instantaneous firing rate of the Poisson neuron between 0 and 100 spk/sec (figure 9.21A). We assume that $s(t)$ and $f_s(t)$ are related through a static sigmoid nonlinearity, $f_s(t) = g_{\alpha,l}(s(t))$ of the form

$$g_{\alpha,l}(y) = \alpha \sqrt{\frac{2}{\pi}} \frac{1}{l} \int_0^y e^{-t^2/2l^2}\, dt. \tag{9.62}$$

Two examples of such sigmoids are illustrated in figure 9.21A, together with the Gaussian distribution of the input stimulus $s(t)$ used in figure 9.18 and in the following. When the nonlinearity is of the form shown in eq. 9.62, the cross-correlation between $s(t)$ and $f_s(t)$ can be computed exactly (using Bussgang's theorem; see Bendat 1990). This is also true for the autocorrelation function of the spike train which is given by[13]

$$R_{xx}(\tau) = R_{f_s f_s}(\tau) + m\delta(\tau)$$
$$= \frac{2\alpha^2}{\pi} \sin^{-1}\left(\frac{R_{ss}(\tau)}{\sigma_s^2 + l^2}\right) + m\delta(\tau), \tag{9.63}$$

where σ_s is the standard deviation in firing rate caused by the random stimulus ($\sigma_s = 20$ Hz in the example of figure 9.21A). Thus it is possible from these equations to compute $|C_{sf_s}(\omega)|$ and $|C_{sx}(\omega)|$ numerically (by using a fast Fourier transform

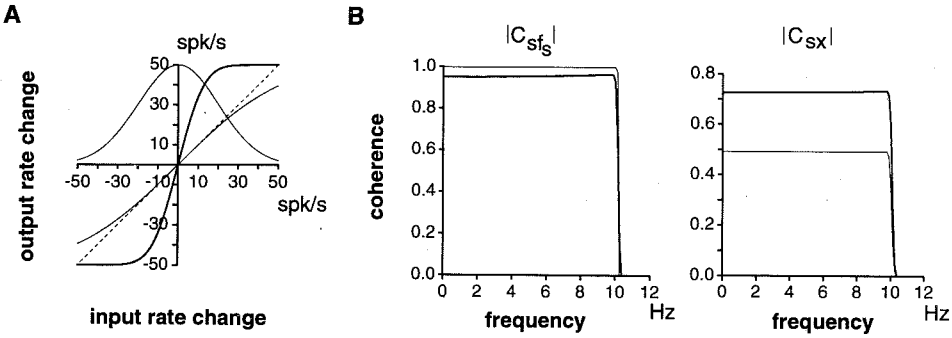

Figure 9.21
Effects of a sigmoid nonlinearity on stimulus encoding in Poisson spike trains. (A) Probability distribution of the Gaussian input is illustrated in units of firing rate changes around the mean rate of the model neuron (50 Hz). In the limit of unit sigmoid gain (the dotted line), no modification occurs between input and output rate changes; this limit is a good approximation for the weak sigmoid nonlinearity (thin line). The thick line illustrates a case where the effect of the nonlinearity is stronger. (B) Magnitude coherence between the instantaneous firing rate and the stimulus ($|C_{sf_s}|$) and between the spike train and the stimulus ($|C_{sx}|$). For $|C_{sf_s}| = 1$, the relation between the stimulus and instantaneous firing rate is a linear one. In both graphs, the thin and thick lines correspond to the thin and thick sigmoids of panel A, respectively. Note that $|C_{sf_s}|$, which measures linearity in stimulus encoding, is closer to 1 for the thin case as compared to the thick case. By contrast, the magnitude coherence $|C_{sx}|$ between stimulus and spike train shows the reversed behavior, indicating a more accurate encoding of the stimulus for the stronger nonlinearity.

algorithm, for instance). The results are shown in figure 9.21B for the two sigmoids of figure 9.21A. Note that in the case of the sigmoid with shallow slope (thin line), the magnitude coherence $|C_{sf_s}(\omega)|$ is almost equal to 1, indicative of a relation between $s(t)$ and $f_s(t)$ that is very close to linear, while the stimulus estimation performance is relatively poor ($|C_{sx}(\omega)| \cong 0.5$ corresponds to $\gamma = 0.14$; see figure 9.18). By increasing the gain of the sigmoid (figure 9.21A, thick line), the linear correlation between $s(t)$ and $f_s(t)$ is slightly diminished (the linear range is clearly reduced as compared to the compression range; see figure 9.21A), while the performance in stimulus estimation is considerably improved ($|C_{sx}(\omega)| \cong 0.72$ corresponding to $\gamma = 0.33$). This is because a large portion of the dynamic firing range of the cell is now devoted to encoding the most likely fluctuations of the stimulus (which would otherwise only cause modulations between ± 20 spk/sec; see figure 9.21A).

Acknowledgments

The research discussed here was supported by the National Science Foundation, the National Institute for Mental Health, and the Sloan Center for Theoretical Neuroscience.

Appendix A: Numerical Estimation Methods

In practice, the quantities defined in the main test, such as the C_V of the interspike interval (ISI) distribution or the power spectrum of the spike train have to be estimated from experimental or simulated data. This appendix provides a short summary of statistical and numerical methods used to obtain such estimates. We will not attempt to cover the subject in depth; extensive treatments may be found in the literature. For a classical reference devoted to the statistical analysis of point processes, see Cox and Lewis 1966; further standard textbooks and reference sources include Oppenheim and Schafer 1989, Press et al. 1992, Anderson 1994, and Ljung 1987.

Mean and Variance of the Interspike Interval Distribution

The mean of the ISI distribution is estimated by the *sample mean*,

$$\hat{t} = \frac{1}{k}\sum_{i=1}^{k} t_i, \tag{9.64}$$

where $t_1, \ldots t_k$ are successively observed interspike intervals. The variance may be estimated from

$$\begin{aligned}\hat{\sigma}_t^2 &= \frac{1}{k}\sum_{i=1}^{k}(t_i - \hat{t})^2 \\ &= \left(\frac{1}{k}\sum_{i=1}^{k} t_i^2\right) - \hat{t}^2.\end{aligned} \tag{9.65}$$

In general, the accuracy of these estimates will depend on the extent of correlations between successive interspike intervals of the spike train (Cox and Lewis 1966; Anderson 1994). The most favorable case is the renewal process because successive intervals are independent. In this case, the variance of $\hat{t}$ is given by σ_t^2/k and decreases linearly with the number of observations from an initial value equal to the variance, σ_t^2, of the ISI distribution. Typically, a few thousand spikes will be sufficient to obtain reliable estimates of $\bar{t}$ and σ_t.

Mean and Variance of the Spike Count

The simplest estimate of the spike count mean and variance on an interval of length T is obtained by subdividing an observation interval T_0 (much longer than T) into $k = T/T_0$ intervals $T_1, \ldots T_k$ of length T. If N_i is the observed count in T_i, we form the estimators

$$\hat{N}(T) = \frac{1}{k}\sum_{i=1}^{k} N_i, \tag{9.66}$$

$$\begin{aligned}\hat{V}(T) &= \frac{1}{k}\left(\sum_{i=1}^{k} N_i - \hat{N}(T)\right)^2 \\ &= \left(\frac{1}{k}\sum_{i=1}^{k} N_i^2\right) - \hat{N}(T)^2.\end{aligned} \tag{9.67}$$

Clearly, this is not the only way of subdividing T_0 into intervals of length T. The intervals $T_1 + (1/2)T, \ldots, T_{k-1} + (1/2)T$ provide $(k-1)$ further observations of N that can be used to form refined estimators for $N(T)$ and $V(T)$, although the improvement will not be as substantial as from independent observations because these new spike counts are correlated to the previous ones. A technique based on this remark consists in subdividing T_0 in $k \cdot r$ intervals $T_1^{sd}, \ldots, T_{kr}^{sd}$ of length T^{sd}, such that $T = r \cdot T^{sd}$. One

then computes a "moving average" estimate of the spike count in all successive intervals of length T by summing r consecutive intervals of length T^{sd}: $N_i = \sum_{j=i}^{r+i} N_j^{sd}$, where N_j^{sd} is the spike count in T_j^{sd}. As a rule of thumb, estimates obtained from eqs. 9.66–9.67 require at least ten times more data, that is, $T_0 \geq 10\,T$, than the largest interval T of interest. Moving average estimates are accurate on intervals that have a length of at most 20%–25% of T_0 (Cox and Lewis 1966).

Power Spectrum and Autocorrelation of the Spike Train

The starting point for power spectral density estimation is the *Wiener-Khinchin formula*,

$$S_{xx}(\omega) = \lim_{T\to\infty} \frac{1}{T}|X_0(\omega)|^2, \tag{9.68}$$

where

$$X_0(\omega) = \int_0^T x_0(t)e^{i\omega t}\,dt, \quad x_0(t) = x(t) - m,$$

which states that the power spectrum can be obtained directly as the squared modulus of the Fourier-transformed series $X_0(\omega)$.

In practice, the occurrence of spikes is recorded with a finite temporal resolution Δt, so that the time series of action potential events is of the form $x = \{x_1, \ldots, x_N\}$, where $x_i = x(t_i)$, $t_i = i \cdot \Delta t (i = 1, \ldots, N)$ and $T = N\Delta t$ is the recording time. The value of x_i is either 0 (if no action potential occurred in the interval $t_i \pm (1/2)\Delta t$) or $1/\Delta t$ (if an action potential occurred in the interval $t_i \pm (1/2)\Delta t$), which is the discrete approximation of the continuous δ-function. The series $\{x_0(t_i)\}_{i=1}^N$ is obtained from $\{x(t_i)\}_{i=1}^N$ by subtracting the mean firing rate, $m = (1/N)\sum_{n=1}^N x_n$.

Ideally, the sampling interval Δt should be sufficiently short to resolve the action potential waveform, thus preventing the aliasing of frequencies above the Nyquist frequency ($f_c = 1/2\Delta t$) below it. In practice, the power spectral density is of interest only for low frequencies (typically, well below 200 Hz) and a sampling interval of 0.5 msec (or even 1 msec) is amply sufficient.

The continuous Fourier transform is approximated by the discrete Fourier transform

$$\hat{X}_0(f_j) = \Delta t \tilde{X}_{0j}, \quad \tilde{X}_{0j} = \sum_{m=1}^{N} x_{0m} e^{2\pi i f_j t_m}, \tag{9.69}$$

where $f_j = \omega_j/2\pi$ takes values at the discrete frequencies $f_j = j/N\Delta t$, $j = -N/2, \ldots, +N/2$ (for N even). An estimator for the power spectral density is given by the *periodogram*

$$\hat{S}(f_j) = \frac{(\Delta t)^2}{T}|\tilde{X}_{0j}|^2, \quad j = -\frac{N}{2}, \ldots, \frac{N}{2}. \tag{9.70}$$

Without any form of averaging, this estimate will be very unreliable. A computationally convenient averaging procedure is to subdivide the observation series into k contiguous segments $l = 1, \ldots, k$, compute the periodogram $\hat{S}_l(f_j)$ separately over each segment, and then average:

$$\hat{S}(f_j) = \frac{1}{k}\sum_{l=1}^{k} \hat{S}_l(f_j). \tag{9.71}$$

A typical example would consist of a spike train sampled at $\Delta t = 0.5$ msec, for which $N = 2{,}048$ points (1.024 sec) are used to compute a single periodogram with a resolution of approximatively $1{,}000/1{,}024 \cong 1$ Hz in the frequency domain.[14] The number of segments needed to obtain a reliable estimate will depend on the firing frequency of the neuron; typically, averaging over 100 segments or 10,000 spikes should yield reasonably accurate results.

The estimate of eq. 9.71 is further improved by multiplying each segment of data with a *window function* prior to Fourier-transforming. This minimizes the boundary effects due to the finite size of the samples. Such a function is the Bartlett window

$$w_k = \begin{cases} \dfrac{2(k-1)}{N-1} & 1 \le k \le \dfrac{N+1}{2}, \\ 2 - \dfrac{2(k-1)}{N-1} & \dfrac{N+1}{2} \le k \le N, \end{cases} \tag{9.72}$$

which peaks at the center of the segment and decreases linearly with distance from the center. Thus, prior to Fourier-transforming, one replaces $(x_{01}, \ldots, x_{0N})$ by $(w_1 x_{01}, \ldots, w_N x_{0N})$.

Finally, the estimate of eq. 9.71 can also be improved by *overlapping* the segments on which the periodograms are computed. In other words, if the first segment consists of data points $x_{01}, \ldots x_{02,048}$, as in the previous example, the second segment should be $(x_{01,024}, \ldots, x_{03,072})$, and so on.

An estimate of the autocorrelation function is obtained from the power spectral density by a straightforward discrete inverse Fourier transformation. Similarly, estimates of cross-correlation functions are obtained using exactly the same procedure outline above, but starting from

$$S_{sx}(\omega) = \lim_{T \to \infty} \frac{1}{T} S(\omega) \bar{X}_0(\omega), \tag{9.73}$$

where the symbol "$\bar{}$" denotes complex conjugation.

First-Order Wiener Kernel, Wiener-Kolmogorov-Filtering

Although the first-order transfer functions of eqs. 9.45 and 9.54 can in principle be estimated directly from the cross-correlation and power spectral density estimates discussed above, this involves a division operation that is very sensitive to noise in the estimates of $S_{sx}(\omega)$ and $S_{ss}(\omega)$ (or $S_{xx}(\omega)$). In the case of the first-order Wiener kernel, this numerically unstable operation may be circumvented by using a white stimulus, so that division by $S_{ss}(\omega)$ at each frequency is replaced by an overall multiplicative constant (see eq. 9.46). One effective way of reducing such noise is to carefully select the sampling step Δt to exclude frequencies higher than those conveyed by the system because they only deteriorate the estimate of the transfer function. (For an example illustrating this point, see tutorial 4 of our MATLAB subroutines; more advanced techniques are discussed in Ljung 1987.) Typically, at least 10,000 spikes are needed to obtain reliable estimates of these transfer functions.

An estimator for the mean square error of eq. 9.55 is obtained from

$$\hat{\varepsilon} = \frac{1}{N} \sum_{i=1}^{N} (s_i - s_{est\,i})^2, \tag{9.74}$$

where s_i is the stimulus value at time point $i\Delta t$ and $s_{est\,i}$ is the estimate obtained by discrete convolution of the Wiener-Kolmogorov filter with $\{x_{0i}\}$. In an optimal situation, the filter h is computed from one data set and the error is estimated from a different data set to avoid a bias of the estimate $\hat{\varepsilon}^2$ toward lower values than the true value ε^2 (this technique is called the "cross-validation method"). In practice, the bias is usually negligible if a sufficiently long data record is used (typically, $|\hat{\varepsilon} - \varepsilon|/\sigma_s \le 0.01$ for data stretches longer than 100 sec) and the same data set may be used to compute the filter and the estimate $\hat{\varepsilon}^2$ (this technique is called the "resubstitution method"). However, the bias can be significant in some cases (see tutorial 6 of our MATLAB subroutines for examples).

Appendix B: MATLAB Interface and Routines

Location

The software as well as the following description may be found on the World Wide Web at http://www.klab.caltech.edu/~gabbiani/signproc.html. The software consists of compressed and archived files directly usable under Unix.

System Requirements

Our routines are written entirely using the programming commands of the MATLAB environment and are therefore independent of the particular platform used (Unix-, Windows-, or MacOS-based systems). In addition to the core MATLAB environment, some analysis routines require the Signal Processing Toolbox. The simulation routines and the graphical interface require the Simulink Toolbox. (The random number generator of the Statistics Toolbox is also used, but could be replaced by a random number generator described in Press et al. 1992.) A fast computer with plenty of memory is recommended.

Software and Data

The software consists of four different parts:

1. *Graphical interface and simulation routines.* This part of the package was written using the S-function formalism (see the Simulink reference manual) and is activated by the **startneuro** M-file (i.e., by entering the command **startneuro** at the MATLAB prompt; see figure 9.22). The subthreshold membrane voltage dynamics of the models described in the main text are linear and were implemented by numerical integration using a fixed time step. This greatly reduced the programming load but leads to relatively slow simulations. (For more sophisticated algorithms, see chapter 14, this volume.) Numerical simulation results were checked by comparison with analytical results (see part 2, "Analysis routines"), but no benchmark tests were performed to assess precisely the numerical accuracy of these routines. We would also like to caution the user that simulation results can be affected by the time step used, the properties of random number generators, and the stability of the linear system simulated.

2. *Analysis routines.* These M-files implement the analysis procedures discussed in the main text. In addition, many theoretical results described there are also implemented in the form of M-files, allowing a direct comparison between simulations and theory. References to the literature are provided in the M-files themselves or through the MATLAB help utility.

3. *Tutorials data.* The spike trains and stimuli data sets resulting from simulations of the tutorials can also be downloaded, thus avoiding having to go through the simulations themselves before performing a data analysis.

4. *Figure notes.* These describe how each figure of the main text was obtained, in the hope that this will clarify the results presented and provide starting points for further simulations.

Notes

1. This description is only accurate if two successive photon events are well separated from each other. It remains valid also for shorter separation times, but the effective number of spikes per incoming photon is reduced (for details, see Tavolacci, Teich, and Saleh, 1981; Saleh and Teich 1985; as well as tutorial 5 in our MATLAB routines).

2. A frequently used approximation uses a fixed T but varies the stimulus to obtain different (N, V) pairs. If, as a function of two variables (f, T), the stochastic properties of the neuron depend only on the product fT, varying the stimulus to increase f is equivalent to varying T. This condition is verified by the integrate-and-fire models with random threshold, provided that the refractory period is set to zero.

3. In the following we ignore the possible occurrence of ties, that is $p_0(n_t) = p_1(n_t)$. The treatment of such cases can be found, for example, in Poor 1994.

4. This terminology arose from early applications of signal detection theory to the performance of radar.

5. This result is known as the "Neyman-Pearson lemma" (Scharf 1991).

6. This result is well known for Poisson spike trains (figure 9.3A) and a general proof for gamma-distributed random threshold noise (figures 9.3B–D) can be found in Gestri 1971. For integrate-and-fire neurons

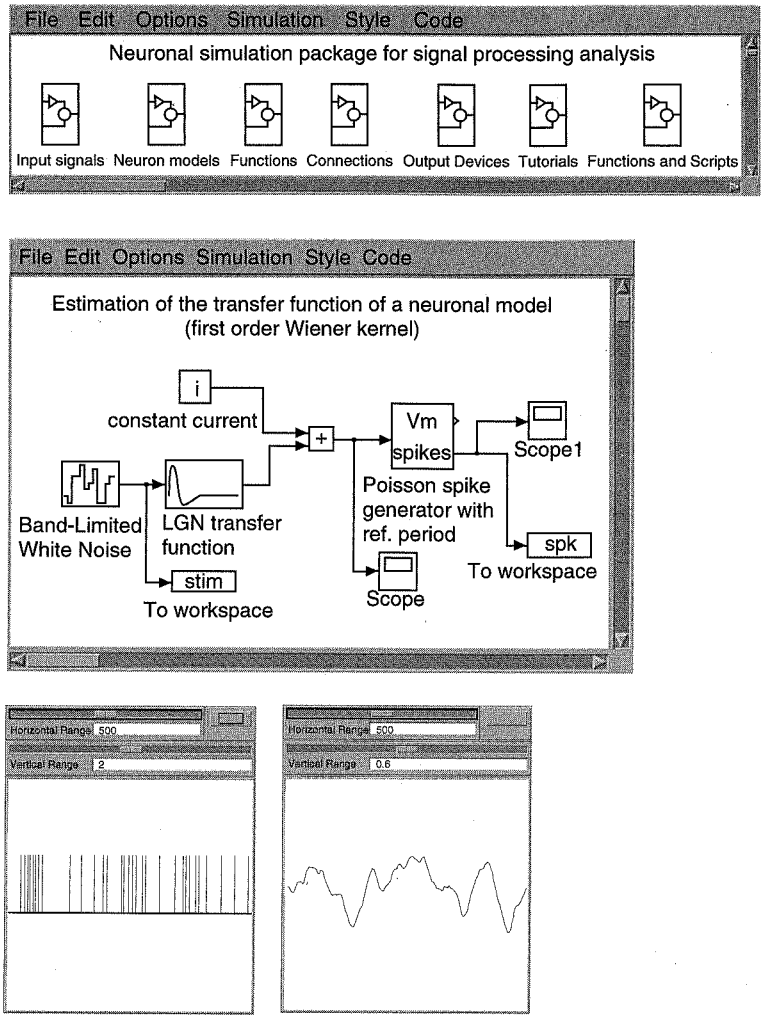

Figure 9.22
Illustration of various windows which constitute the software package for analysis of spike trains using signal processing methods. The top window can be called directly from the main MATLAB workspace window and contains several icons which can be accessed by double-clicking on them. "Input signals," "Neuron models," "Functions," "Connections," and "Output devices" contain building blocks that allow users to constitute models such as the one shown in the middle window. This window is one of the tutorials that can be accessed by double-clicking on the "Tutorials" icon, while double-clicking on the "Functions and Scripts" icon accesses help for the analysis procedures. Spike trains and stimulus vectors, such as the ones shown in the bottom two windows, can be stored directly in MATLAB variables and analyzed using the functions described by the "Functions and Scripts" icon.

(figure 9.3E), eq. 9.37 was proven in Knight 1972a. In fact, the encoding of analog time-varying signals in binary spikes of integrate-and-fire neurons is equivalent to the engineering coding scheme of *integral pulse frequency modulation* (Bayly 1968; Zeevi and Bruckstein 1977).

7. This equation holds exactly for the Poisson model of figure 9.3A (because once the mean stimulus $s_0(t)$ is specified, spikes are generated independently of each other), but will usually not be satisfied exactly by more general models.

8. This is a very strong assumption. Methods to generate such ensembles are described in Marmarelis and Marmarelis 1978.

9. An extreme (and academic) example is $g(y) = y^2$, so that $c = 0$ in eq. 9.48 and the linear estimator is at chance level.

10. Such procedures also exist for other stimulus ensembles (Palm and Poggio 1978; Victor and Shapley 1980).

11. The signal-to-noise ratio can also been normalized to take values from 0 to infinity by subtracting 1; see Bialek et al. 1991 and Gabbiani 1996.

12. The magnitude coherence $|C_{sf_s}(\omega)|$ is also difficult to measure experimentally as compared to $|C_{sx}(\omega)|$.

13. This famous result is originally due to R. F. Baum (1957). More recent derivations use a result due to Price (1958).

14. The number of points N is usually chosen to be a power of 2 so that fast Fourier transform algorithms can be applied.